



# Tidal mixing of estuarine and coastal waters in the western English Channel is a control on spatial and temporal variability in seawater CO<sub>2</sub>

Richard P. Sims<sup>1</sup>, Michael Bedington<sup>2</sup>, Ute Schuster<sup>3</sup>, Andrew J. Watson<sup>3</sup>, Vassilis Kitidis<sup>2</sup>, Ricardo Torres<sup>2</sup>, Helen S. Findlay<sup>2</sup>, James R. Fishwick<sup>2</sup>, Ian Brown<sup>2</sup>, and Thomas G. Bell<sup>2</sup>

<sup>1</sup>Department of Geography, University of Calgary, Calgary, T2N 1N4, Canada

<sup>2</sup>Plymouth Marine Laboratory, Plymouth, PL1 3DH, UK

<sup>3</sup>Department of Geography, University of Exeter, Exeter, EX4 4QE, UK

**Correspondence:** Richard P. Sims (r.sims2@exeter.ac.uk) and Thomas G. Bell (tbe@pml.ac.uk)

Received: 21 June 2021 – Discussion started: 1 July 2021

Revised: 2 February 2022 – Accepted: 14 February 2022 – Published: 23 March 2022

**Abstract.** Surface ocean carbon dioxide (CO<sub>2</sub>) measurements are used to compute the oceanic air–sea CO<sub>2</sub> flux. The CO<sub>2</sub> flux component from rivers and estuaries is uncertain due to the high spatial and seasonal heterogeneity of CO<sub>2</sub> in coastal waters. Existing high-quality CO<sub>2</sub> instrumentation predominantly utilises showerhead and percolating style equilibrators optimised for open-ocean observations. The intervals between measurements made with such instrumentation make it difficult to resolve the fine-scale spatial variability of surface water CO<sub>2</sub> at timescales relevant to the high frequency variability in estuarine and coastal environments. Here we present a novel dataset with unprecedented frequency and spatial resolution transects made at the Western Channel Observatory in the south-west of the UK from June to September 2016, using a fast-response seawater CO<sub>2</sub> system. Novel observations were made along the estuarine–coastal continuum at different stages of the tide and reveal distinct spatial patterns in the surface water CO<sub>2</sub> fugacity ( $f\text{CO}_2$ ) at different stages of the tidal cycle. Changes in salinity and  $f\text{CO}_2$  were closely correlated at all stages of the tidal cycle and suggest that the mixing of oceanic and riverine endmembers partially determines the variations in  $f\text{CO}_2$ . The correlation between salinity and  $f\text{CO}_2$  was different in Cawsand Bay, which could be due to enhanced gas exchange or to enhanced biological activity in the region. The observations demonstrate the complex dynamics determining spatial and temporal patterns of salinity and  $f\text{CO}_2$  in the region. Spatial variations in observed surface salinity were used to val-

idate the output of a regional high-resolution hydrodynamic model. The model enables a novel estimate of the air–sea CO<sub>2</sub> flux in the estuarine–coastal zone. Air–sea CO<sub>2</sub> flux variability in the estuarine–coastal boundary region is influenced by the state of the tide because of strong CO<sub>2</sub> outgassing from the river plume. The observations and model output demonstrate that undersampling the complex tidal and mixing processes characteristic of estuarine and coastal environment biases quantification of air–sea CO<sub>2</sub> fluxes in coastal waters. The results provide a mechanism to support critical national and regional policy implementation by reducing uncertainty in carbon budgets.

## 1 Introduction

The ocean has taken up about a quarter of anthropogenic carbon dioxide (CO<sub>2</sub>) emissions to date, absorbing approximately 2.5 Pg C yr<sup>-1</sup> (Friedlingstein et al., 2019). Global observations of the partial pressure of CO<sub>2</sub> in seawater ( $p\text{CO}_2$ ) are stored in the Surface Ocean CO<sub>2</sub> Atlas (SOCAT) (<https://www.socat.info/>, last access: 20 March 2022) (Bakker et al., 2016). The latest version of SOCAT (v2021) contains ~32.7 million  $p\text{CO}_2$  measurements, with the majority ( $\gtrsim 75\%$ ) of data collected in the open ocean (Laruelle et al., 2018). The carbon cycle in continental shelf waters has been extensively studied in recent years (Laruelle et al., 2018; Robbins et al., 2018; Kahl et al., 2017; Ahmed and

Else, 2019; Laruelle et al., 2017b; Kitidis et al., 2019; Fenel et al., 2019). Whilst the surface area of coastal, estuarine and continental shelf waters makes up 7.5 % of global waters ( $\sim 2.7 \times 10^7 \text{ km}^2$ ) (Cai, 2011), continental shelves alone have been shown to take up a substantial proportion 0.20–0.25  $\text{Pg C yr}^{-1}$  (8 %–10 %) of global ocean uptake (Laruelle et al., 2018, 2014; Chen et al., 2013; Cai, 2011; Bauer et al., 2013). Estuaries are net heterotrophic and thus typically oversaturated with  $p\text{CO}_2$  with respect to the atmosphere (Laruelle et al., 2017a; Frankignoulle et al., 1998). The global air–water  $\text{CO}_2$  flux from estuaries is thus into the atmosphere, and this flux is currently perceived to roughly offset the  $\text{CO}_2$  uptake by the continental shelves (Cai, 2011; Borges et al., 2006). However, the global estuarine air–water  $\text{CO}_2$  flux remains highly uncertain, with estimates ranging from 0.09 to 0.78  $\text{Pg C yr}^{-1}$  (Cai, 2011; Laruelle et al., 2010; Chen and Borges, 2009; Chen et al., 2013; Resplandy et al., 2018; Roobaert et al., 2019).

Estuaries and rivers around major ports and harbours are deep and easily accessed with large research vessels. However, many estuaries are shallow and/or have irregular topography. Navigating shallow estuaries safely, particularly at low tide, is not always possible for many ocean-going research vessels, such that mapping the  $p\text{CO}_2$  is challenging. The observations of  $p\text{CO}_2$  included in SOCAT from upper estuarine waters come from a limited number of research vessels that are typically small ( $\sim 25 \text{ m}$  long) and have shallow ( $\sim 3 \text{ m}$ ) draughts. Transects of large rivers and estuaries by shallow-bottom boats identify a  $\text{CO}_2$  concentration gradient between the mouth and source, with high  $p\text{CO}_2$  ( $\sim 10\,000 \text{ ppm}$ ) up-river and  $p\text{CO}_2$  levels similar to seawater close to the river mouth (Borges et al., 2018; Joesoef et al., 2015; Macklin et al., 2014; Bozec et al., 2012; Volta et al., 2016; Cai, 2011; Jeffrey et al., 2018b). Assessment of  $p\text{CO}_2$  in inland waters, determined from measurements of total alkalinity (TA) and dissolved inorganic carbon (DIC), is also highly uncertain due to limited carbonate buffering capacity at low pH and because acids in terrestrial organic matter make an unknown contribution to the TA anions (Abril et al., 2015).

The zone where estuarine waters meet coastal waters is a physically dynamic system influenced by riverine outflow, winds, waves and tidal cycles; hence,  $p\text{CO}_2$  is likely to vary where estuarine water and continental shelf water interact, yet there has been relatively little attention given to air–water  $\text{CO}_2$  fluxes in this zone (Cai, 2011). Increased research effort over the past decade has shown that many processes are important in this zone (Cai et al., 2021; Ward et al., 2017; Shen et al., 2019). One holistic modelling study has tried to understand the coastal system in eastern North America, encompassing tidal wetlands, estuaries and continental shelves (Najjar et al., 2018). The study demonstrated that, despite estuaries representing  $< 10 \%$  of the domain area, interactions with shelf seas must be considered as the estuarine waters gave off more  $\text{CO}_2$  than the shelves drew down. Eulerian studies in the estuarine zone have identified large tidal signals in

$p\text{CO}_2$  with data collected from research vessels (Borges and Frankignoulle, 1999; Jeffrey et al., 2018a) and from moorings or fixed sites (Dai et al., 2009; Jeffrey et al., 2018a; Li et al., 2018; Bakker et al., 1996; Call et al., 2015; Ferrón et al., 2007; Santos et al., 2012).  $p\text{CO}_2$  levels at the mouth of different rivers have been observed to co-vary with changes in river flow rate and with the tidal cycle (Ribas-Ribas et al., 2013; Canning et al., 2021; Najjar et al., 2018; Frankignoulle et al., 1996). Underway  $\text{CO}_2$  measurements along transects have been made (Hales et al., 2005) but have not been regularly repeated through the transitional zone where estuaries connect with continental shelf waters.

Here we present weekly surface water  $f\text{CO}_2$  observations along a  $< 8 \text{ km}$  transect from estuarine waters into continental shelf waters in the western English Channel between April and September 2016 (Fig. 1). The  $\text{CO}_2$  measurement system was capable of high spatial ( $\sim 0.2 \text{ km}$ ) and temporal resolution ( $\sim 48 \text{ s}$ ), revealing substantial variations in surface  $f\text{CO}_2$ . Our aim was to examine in detail the transition zone between rivers, estuaries and the coastal zone in order to investigate variations in surface  $\text{CO}_2$  and potential drivers of this variation. We then used the observed relationship in the  $\text{CO}_2$  and salinity data together with the output of a high-resolution hydrodynamic model of the estuary and nearshore region to estimate the spatial heterogeneity in  $f\text{CO}_2$  and air–water  $\text{CO}_2$  flux.

## 2 Study location and physical setting

This study was conducted in the English Channel off the coast of Plymouth (south-west UK) at the Western Channel Observatory (WCO, see Fig. 1a), which includes the oceanographic station L4 ( $50.251^\circ \text{ N}$ ,  $4.221^\circ \text{ W}$ ; Smyth et al., 2010a) and the Penlee Point Atmospheric Observatory (PPAO,  $50.319^\circ \text{ N}$ ,  $4.193^\circ \text{ W}$ ; Yang et al., 2019, 2016) among other routine monitoring activities and assets. The PPAO is a coastal land-based observatory on the Rame Head peninsula at the entrance to the Plymouth Sound. Station L4 is a coastal site  $\sim 8 \text{ km}$  from PPAO and is a focal point of the ongoing WCO time series.

L4 is seasonally stratified between late April and early October (Smyth et al., 2010b). The onset of stratification typically drives a diatom-dominated spring bloom in early April. Nitrogen limitation later in the year favours a summertime dominance of smaller plankton (Widdicombe et al., 2010). A prominent feature of the coastal region around WCO is the coastal/tidal current that entrains buoyant freshwater from the River Tamar outflow with prominent frontal features (Uncles and Torres, 2013). The River Tamar is a large source of freshwater to the region despite being a relatively small river (Uncles et al., 2015). The coastal current moves along the west coast of Plymouth Sound adjacent to the Plymouth Breakwater and toward PPAO before following the coastline towards the Rame Head peninsula (Uncles et al., 2015; Sid-

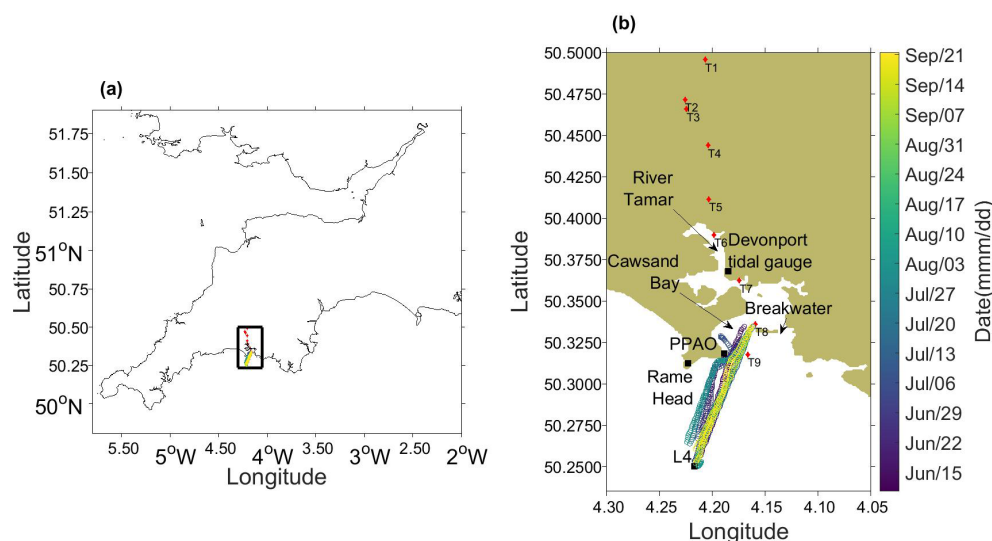


**Figure 1.** (a) Map of the south-west of the England Western Channel Observatory (WCO) and study area (black rectangle). (b) Breakwater to L4 transects for the 15 transects made with the RV *Plymouth Quest* (coloured circles). Ship tracks are coloured by date between 10 June and 21 September 2016. The River Tamar, Devonport tidal gauge station, Plymouth Breakwater, Cawsand Bay, PPAO, Rame Head and station L4 are marked. Transect sites T1–T9 are shown as red diamonds.

dorn et al., 2003). The River Tamar is known to occasionally influence L4. For example salinity reductions of  $\sim 0.5$  have been observed after several days of rainfall led to elevated river discharge rates (Rees et al., 2009).

The annual cycle of L4 surface water  $p\text{CO}_2$  is mainly determined by biological activity, with the spring bloom depleting  $p\text{CO}_2$  in April and May (Torres et al., 2020). Seawater  $p\text{CO}_2$  increases to pre-bloom levels throughout the summer and is at equilibrium or slightly oversaturated with respect to the atmosphere in the autumn and winter (Kitidis et al., 2012; Marrec et al., 2013). Surface water  $p\text{CO}_2$  decreases with distance offshore at all times of the year, with the greatest variability within 10 km of the coast (Kitidis et al., 2012). Changes in surface  $p\text{CO}_2 > 40$  ppm have been observed during a 24 h Eulerian study at L4 (Litt et al., 2010). Direct methane flux measurements made at the PPAO indicate that the waters around the Rame Head peninsula are influenced by the interaction between tidal cycles and the Tamar freshwater outflow (Yang et al., 2016).

## 2.1 Methods

### 2.1.1 Sampling approach

Transects between the breakwater in the Plymouth Sound and station L4 were conducted weekly where possible during the study period (Fig. 1b). Transects took place between 09:00 and 15:00 BST (UTC+1) using the RV *Plymouth Quest*. Fifteen transects were conducted on 12 non-sequential days between 10 June and 21 September 2016. RV *Plymouth Quest* takes  $\sim 40$  min to travel directly to L4 during transects, except during a number of voyages when

the ship was redirected into Cawsand Bay and/or closer to the PPAO. The underway seawater system on the ship has an intake at 3 m depth, supplying seawater for measurements of  $p\text{CO}_2$ , sea surface temperature (SST) and surface salinity (SBE45; Sea-Bird Scientific, USA). The underway system is turned off when the ship is shoreside of the breakwater to reduce the risk of heavy biofouling and the intake of large quantities of sediment and coastal debris.

A rigid inflatable boat (*PML Explorer*) was used to sample the River Tamar on the 1 October 2014. SST and salinity were measured with a portable CTD package (SeaCat CTD 19plus; Sea-Bird Scientific), and seawater was sampled at nine stations along a  $\sim 25$  km transect between the breakwater and Calstock slip (T1, Fig. 1b,  $50^\circ 29.732' \text{ N}$ ,  $4^\circ 12.408' \text{ W}$ ). Seawater was collected for laboratory analysis of total alkalinity (TA) and dissolved inorganic carbon (DIC) following the best practice (SOP 1 of Dickson et al., 2007). The salinity (35.16) and  $p\text{CO}_2$  (410.93 ppm) were measured by the RV *Plymouth Quest* on the 29 September 2014 at station L4.

### 2.1.2 Seawater $\text{CO}_2$ and carbonate system analyses

Two independent  $\text{CO}_2$  systems with different equilibrators designs were used to measure seawater  $\text{CO}_2$  on the RV *Plymouth Quest*. The PML-Dartcom Live  $p\text{CO}_2$  system (Dartcom Systems Ltd, UK) is permanently installed to measure ocean surface  $\text{CO}_2$  at L4 and utilises a vented showerhead equilibrator with an equilibration time of 8 min (four e-folding times). This was set up with a sampling frequency of 27 min (Kitidis et al., 2012). The showerhead system also measured atmospheric  $p\text{CO}_2$  every 27 min. Addition-

ally, a high-frequency and high-resolution membrane CO<sub>2</sub> system (Sims et al., 2017) was installed during the study period. This system utilises a membrane equilibrator (Hales et al., 2004) with a fast response time of 48 s (two *e*-folding times) and has a high sampling frequency (1 Hz). Both CO<sub>2</sub> systems were calibrated with the same secondary standards (263.04 and 483.36 ppm), traceable to WMO standards by cross calibration at PML against National Oceanic and Atmospheric Administration Global Monitoring Laboratory (NOAA GML, USA) certified standards (244.91, 388.62 and 444.40 ppm). The membrane system was calibrated pre- and post-voyage (~ 4–5 h apart), and the showerhead system was calibrated hourly while the underway system was running.

The membrane and Dartcom systems used non-dispersive infrared gas analysers (model 840B and 7000, respectively; LI-COR, Inc., USA) to measure gas phase CO<sub>2</sub> mixing ratio ( $\alpha$ CO<sub>2</sub>) in the equilibrated gas exiting the membrane or showerhead equilibrators. The fugacity of CO<sub>2</sub> inside the equilibrator ( $f$ CO<sub>2(eq)</sub>) and the fugacity of CO<sub>2</sub> in seawater ( $f$ CO<sub>2(sw)</sub>) were calculated using measured SST, surface salinity, equilibrator pressure and equilibrator temperature, using equations listed in SOP 5 (Dickson et al., 2007). Lag-time correlation analysis between SST and the equilibrator temperature identified that a -79 s adjustment should be made to the  $f$ CO<sub>2</sub> measurement time. The  $f$ CO<sub>2</sub> time adjustment accounted for the time taken for water to enter the seawater intake beneath the hull of the ship and arrive at the showerhead and membrane equilibrators.

The flux ( $F$ ) of CO<sub>2</sub> (mmol m<sup>-2</sup> d<sup>-1</sup>) is computed following Wanninkhof (2014):

$$F_{(\text{sea-air})} = k_w k_0 \Delta f \text{CO}_2 \text{SF}. \quad (1)$$

$k_w$  is the water phase gas transfer velocity (cm h<sup>-1</sup>; Eq. 2),  $k_0$  is the solubility of CO<sub>2</sub> in seawater (mol L<sup>-1</sup> atm<sup>-1</sup>) from Weiss (1974),  $\Delta f$ CO<sub>2</sub> is the difference in fugacity between the atmosphere and ocean ( $\mu$ atm; Eq. 3), and SF is a scaling factor of 0.24 to express the result flux  $F$  in units of mmol m<sup>-2</sup> d<sup>-1</sup>.

The gas transfer velocity is computed following Nightingale et al. (2000):

$$k_w = (0.222(U_{10})^2 + 0.333(U_{10})) (Sc/660)^{-1/2}, \quad (2)$$

where  $U_{10}$  is the mean wind speed at 10 m height, and for neutral conditions,  $Sc$  is the scaling by unitless Schmidt number of 660 (Wanninkhof, 2014).  $U_{10}$  measurements were taken from the L4 buoy (Smyth et al., 2010a).

$\Delta f$ CO<sub>2</sub> is here defined as the difference between the seawater interface fugacity and the fugacity of air:

$$\Delta f \text{CO}_2 = f \text{CO}_{2(\text{sw})} - f \text{CO}_{2(\text{air})}. \quad (3)$$

To account for the cool and salty layer at the atmosphere ocean interface, -0.17 °C and +0.1 were added to the in situ temperature and salinity when calculating seawater  $f$ CO<sub>2</sub>

at the interface and for the estimation of air–sea CO<sub>2</sub> flux (Woolf et al., 2019).

TA samples were measured by open-cell potentiometric titration with 0.1 M hydrochloric acid on a total alkalinity titrator (model AS-ALK2; Apollo SciTech, Inc. USA) following SOP 3b in Dickson et al. (2007). DIC was measured using an Apollo SciTech DIC analyser (model AS-C3; Apollo SciTech, Inc., USA) following SOP 2 in Dickson et al. (2007) and Sabine et al. (2007). Samples were acidified with excess 10 % phosphoric acid, and nitrogen gas was then used to transfer liberated CO<sub>2</sub> to an infrared gas analyser (LI-COR model 7000, LI-COR, Inc., USA). These two measurement systems are described in more detail in Kitidis et al. (2017).  $f$ CO<sub>2</sub> was calculated from TA and DIC using CO2SYS in MATLAB (Van Heuven et al., 2011) with the carbonic acid dissociation constants of Mehrbach (1973) re-fit by Dickson and Millero (1987) and the hydrogen sulfate dissociation constant of Dickson (1990).

### 2.1.3 Numerical model

The hydrodynamics of the WCO were modelled following Uncles et al. (2020) using an implementation of the Finite-Volume Community Ocean Model (FVCOM; Chen et al., 2003). The model domain (~ 49.7 to 50.6° N and ~ 4.8 to 3.8° W) encompasses station L4, PPAO, Plymouth Sound and the estuary of the River Tamar including its major tributaries. FVCOM utilises an unstructured grid consisting of a mesh of variable resolution triangles, which allows the representation of complex coastlines and higher resolution in areas of interest whilst remaining computationally feasible. The resolution of the model is ~ 600 m at L4, becoming finer towards the PPAO and Plymouth Sound (~ 85 m), with the highest resolution around the upper River Tamar channel (~ 40 m). The vertical system is terrain-following sigma coordinates with 24 equally spaced layers. Horizontal mixing is parameterised through the (Smagorinsky, 1963) scheme and vertical turbulence closure through an updated version of the MY 2.5 scheme (Mellor and Yamada, 1982), with mixing coefficients of 0.2 and  $1 \times 10^{-5}$ , respectively.

Water depth within the model domain uses the EMODNET bathymetry product with a nominal resolution of 1/16°. In the estuary and nearshore areas (< 20 m depth) the data have been complemented with local data sources of lidar, single and multi-beam surveys accessed through the Channel Coastal Observatory (CCO, <https://www.channelcoast.org/>, last access: March 2015). The CCO data were re-projected from their original projection (OSGB) to WGS84 and concatenated and averaged into a 20 m regular grid using the Generic Mapping Tools (GMT 5.3.2) software (<http://gmt.soest.hawaii.edu/doc/5.3.2/gmt.html>, last access: March 2015). The merged dataset was processed using the Regional Ocean Modelling System (ROMS) toolbox for bathymetry processing downloaded from <https://github.com/dcherian/ROMS> (last access: March 2015). The scattered

bathymetry was interpolated to 25 m and smoothed iteratively to achieve a Haney number less than 2 (Haney, 1991).

Lateral boundary conditions are provided as a one-way direct nesting at hourly resolution from a larger FVCOM model covering the west UK shelf (Cazenave et al., 2016). The surface atmospheric forcing is from the NCEP GFS 6-hourly historical product, which is downscaled to  $\sim 3$  km resolution using a triple nested implementation of the Weather Research and Forecasting (WRF) model (Skamarock et al., 2008). The freshwater input flux for 11 rivers in the domain was obtained from daily river gauge data from the National River Flow Archive (<https://nrfa.ceh.ac.uk>, last access: December 2016). The temperature of freshwater inputs was determined using a regression model on the WRF 2 m air temperature, which was trained on temperature records from the UK Environment Agency's Surface Water Temperature Archive (Orr et al., 2010) and data from the Wessex Rivers Trust.

The model was run for the period between March 2016 and November 2016, with instantaneous values output hourly. Only the uppermost layer of the FVCOM output is used in the analysis below. The thickness of this layer varies between 0.05 and 5 m across the domain (because the model uses terrain-following coordinates), and the significance of this and how it relates to the 3 m underway measurement and air–sea  $\text{CO}_2$  fluxes is discussed below.

### 3 Results

#### 3.1 Showerhead vs. membrane comparison

Surface  $f\text{CO}_2$  was measured for several hours, while RV *Plymouth Quest* was stationary at L4 in between outbound and return transects. The showerhead system sampled continuously from the fixed seawater intake (3 m depth). The membrane equilibrator system was switched to sample via tubing from a near-surface ocean profiler (Sims et al., 2017) when at L4 (Fig. S1 in the Supplement). The two  $\text{CO}_2$  systems showed good agreement when the surface ocean profiler was between 2.5 and 3.5 m, despite sampling slightly different water through different tubing (Fig. 2). The mean residual was  $2.77 \mu\text{atm}$  and the RMSE was  $6.9 \mu\text{atm}$  when sampling on station (Fig. 2); this is similar to the  $\pm 2 \mu\text{atm}$  difference that has been observed during other seawater  $\text{CO}_2$  intercomparison exercises (Körtzinger et al., 2000; Ribas-Ribas et al., 2014; Jiang et al., 2008). The  $\text{CO}_2$  systems both sampled from the underway seawater supply of the ship during the L4 to breakwater transects, and  $f\text{CO}_2$  was estimated from  $p\text{CO}_2$  using the underway SST and salinity. The 11 coincident  $f\text{CO}_2$  measurements during the transects had a mean residual of  $2.88 \mu\text{atm}$  and a RMSE of  $27.1 \mu\text{atm}$  (Fig. 2). The largest differences between the  $\text{CO}_2$  systems tend to occur when the ship was not on station at L4.

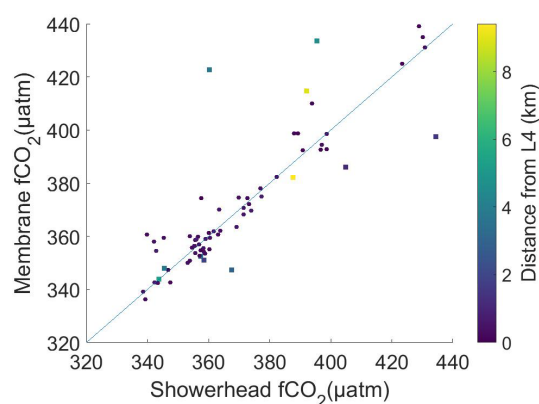


**Figure 2.** Comparison of coincident seawater  $f\text{CO}_2$  measurements made using membrane and showerhead equilibrator systems on the RV *Plymouth Quest*. Both systems sampled from the underway seawater supply during transects between L4 and the Plymouth Breakwater (filled squares). The ship was stationary for long periods ( $> 1$  h) at L4 (filled circles). The membrane equilibrator system was switched at L4 to tubing connected to a near-surface profiler (Sims et al., 2017) while the showerhead system continued to sample from the underway supply. Data points are coloured as a function of distance from L4 (km). The 1 : 1 line represents perfect agreement and is shown for reference.

#### 3.2 Spatial and temporal variation in salinity, SST and $f\text{CO}_2$

Sea surface salinity at L4 during the June to October study period does show small variation (mean  $\pm$  SD =  $35.15 \pm 0.08$ ; Fig. 3a). The L4 salinity range during the study period is within the range of previous years (Smyth et al., 2010b). L4 salinity decreased intermittently, with a maximum reduction of 0.68 on 9 August. The salinity measurements at L4 contrast with the large variability in breakwater salinity during the study period (34.17–35.23). The average salinity difference between the breakwater and L4 is 0.36. The salinity ranges observed at L4 and at the breakwater are similar to model results during a tidal cycle (Uncles et al., 2015).

Coastal SSTs (Fig. 3b) followed the seasonal warming pattern slowly increasing from  $13.9^\circ\text{C}$  on 10 June to  $16.7^\circ\text{C}$  on 21 September. The warming trend was in broad agreement with SST trends observed during previous years (Smyth et al., 2010b). The SST variation along each transect was typically small ( $< 1^\circ\text{C}$ ) compared to the SST change over the study period ( $2.8^\circ\text{C}$ ). The smallest temperature difference between L4 and the breakwater ( $0.025^\circ\text{C}$ ) occurred on 15 September. The largest temperature differences occurred during early summer ( $1.20$ ,  $0.63$ ,  $0.59$  and  $0.65^\circ\text{C}$  on 10, 15, 22 and 30 June, respectively).

L4 surface  $f\text{CO}_2$  increased from 355 to  $420 \mu\text{atm}$  between 10 June and 21 September (Fig. 3c). The average  $f\text{CO}_2$  difference between L4 and the breakwater was  $20 \mu\text{atm}$ . Abrupt

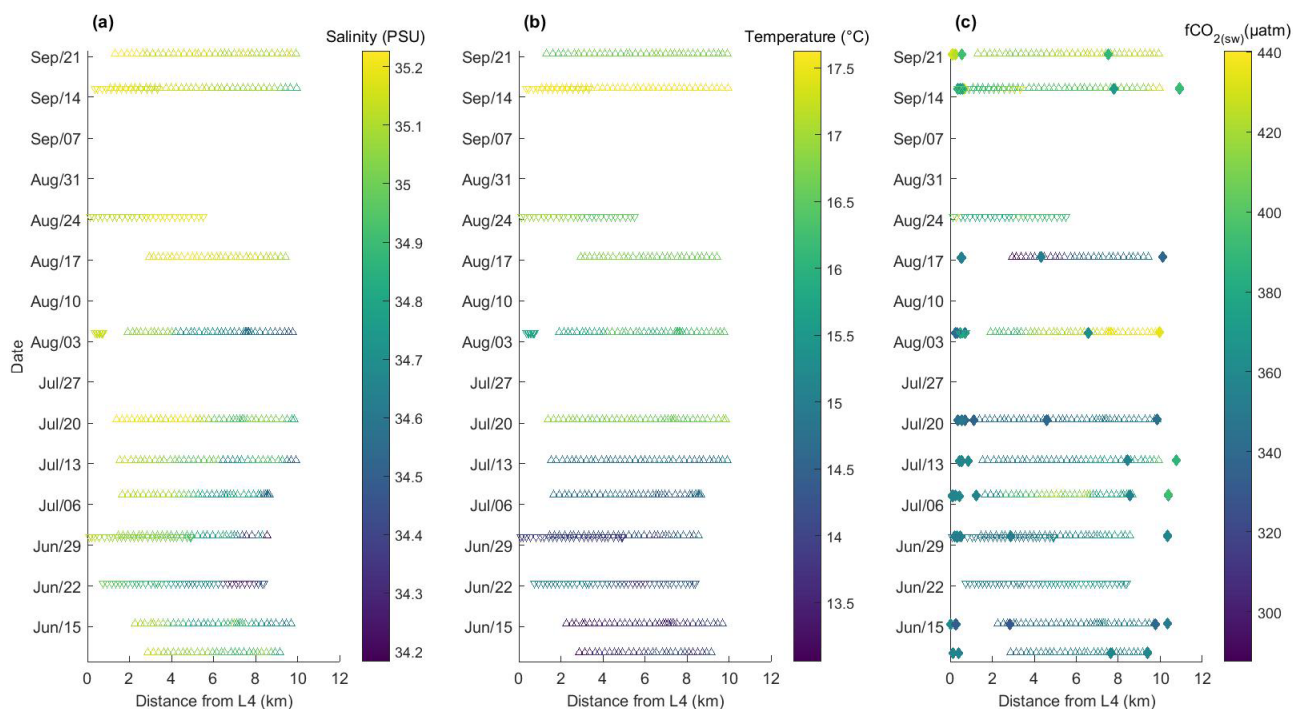


**Figure 3.** Surface water transects by RV *Plymouth Quest* between Plymouth Breakwater and station L4 from 10 June to 21 September 2016. Plotted are (a) salinity, (b) temperature and (c)  $f\text{CO}_2$  as a function of distance from L4. Outbound transects are shown as downwards triangles, and inbound transects are shown as upwards triangles for salinity, temperature and membrane equilibrator  $f\text{CO}_2$  (sampling period = 0.5 min). Showerhead equilibrator  $f\text{CO}_2$  observations are denoted by filled diamonds.

changes in  $f\text{CO}_2$  were observed along the transects, generally close to the breakwater (> 4 km from the L4 station).  $f\text{CO}_2$  in waters within 4 km of the breakwater ranged between 338 and 440  $\mu\text{atm}$  during the study period.  $f\text{CO}_2$  measurements within 2 km of the PPAO also varied considerably during some of the transects; for example,  $f\text{CO}_2$  varied between 337 and 434  $\mu\text{atm}$  during the transect past the PPAO on 7 July. The variability in membrane equilibrator  $f\text{CO}_2$  measurements agreed with previous observations in the region (Kitidis et al., 2012).

When transects were ordered by stage along the 12 h tidal cycle, the spatial variability in salinity transects (Fig. S2 in the Supplement) appeared to correspond to the different stages of the tidal cycle. Temperature and  $f\text{CO}_2$  transects can be found in the Supplement (Figs. S3 and S4). We divided our transect data according to the stage in the tidal cycle (determined from the Devonport tidal gauge station; 50.368° N, -4.185° W; Fig. 1b). Transects were characterised by the time elapsed since the last period of low water (i.e. LW + X h) using the time at the midpoint of each transect.

Four categories were used, corresponding to 3 h tidal periods: low water (LW + 0 h), flooding tide (LW + 3 h), high water (LW + 6 h) and ebbing tide (LW + 9 h). Four transects are used below to exemplify the relationship between the dif-

ferent stages of the tidal cycle and the spatial variation in  $f\text{CO}_2$  (Figs. 4–7).

### 3.3 Example transects

The transect on 7 July (low water, LW + 0 h) began at L4 and headed inland (Fig. 4). Salinity was 35.1 close to L4 and declined along the transect. The low salinity was directly north of PPAO (34.7) and in the shallow waters of Cawsand Bay (north of PPAO, 35.5). SST was warmest near L4 and in the relatively shallow Cawsand Bay. The river water was cooler than the L4 seawater, and there was a negative gradient (0.55 °C) into Cawsand Bay.  $f\text{CO}_2$  was lowest ( $\sim 360 \mu\text{atm}$ ) when near to L4 and highest ( $\sim 430 \mu\text{atm}$ ) immediately south of PPAO.  $f\text{CO}_2$  to the north of PPAO in Cawsand Bay was  $\sim 390 \mu\text{atm}$ , which is lower than waters south of PPAO.

The data collected on 15 June are an example from a flooding tide transect (LW + 3 h, Fig. 5). Salinity was 35.1 in waters close to L4 and decreased toward PPAO and the breakwater (34.7 minimum). The River Tamar plume was warmer than coastal waters in July. SST was highest ( $\sim 14.1 \text{ °C}$ ) close to the breakwater, and the coldest water along the transect (13.3 °C) was near to L4. The difference in  $f\text{CO}_2$  between L4 and the breakwater was  $\sim 18 \mu\text{atm}$ , with higher  $f\text{CO}_2$  (353  $\mu\text{atm}$ ) in the warm, low-salinity water close to the breakwater.

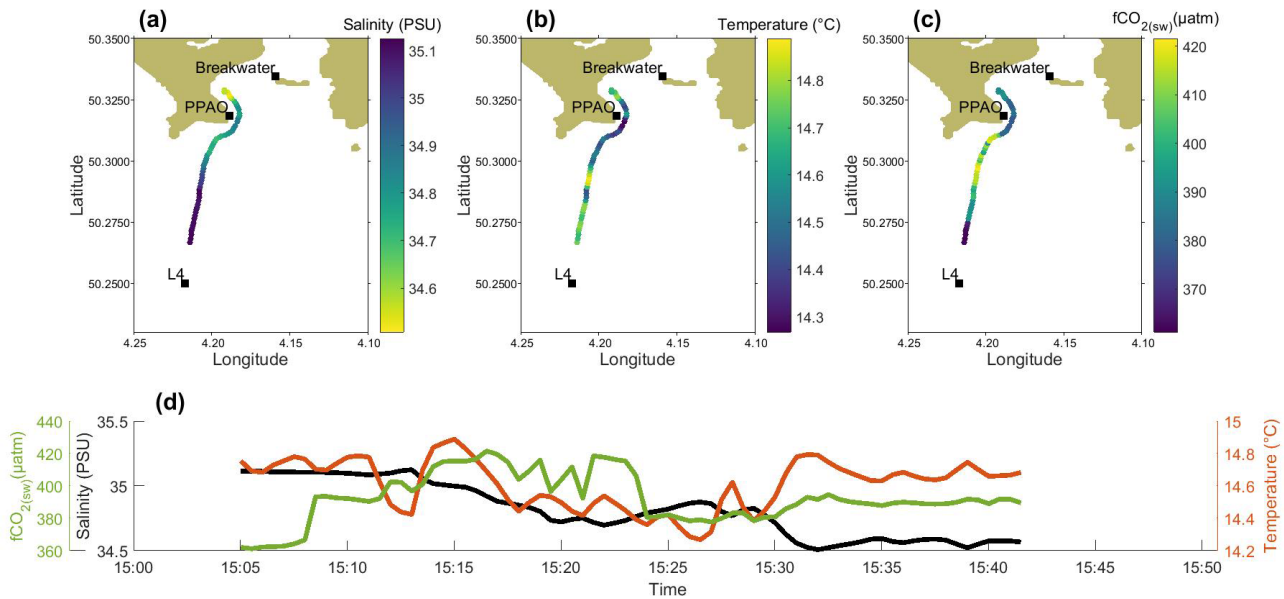


**Figure 4.** Example of a low water transect (transect midpoint = LW + 0.5 h). Surface measurements of salinity, temperature and  $f\text{CO}_2$  represented spatially (a–c) and as a time series (d) from station L4 toward the coast. Data were collected aboard RV *Plymouth Quest* on 7 July 2016 (filled circles, data every 30 s).

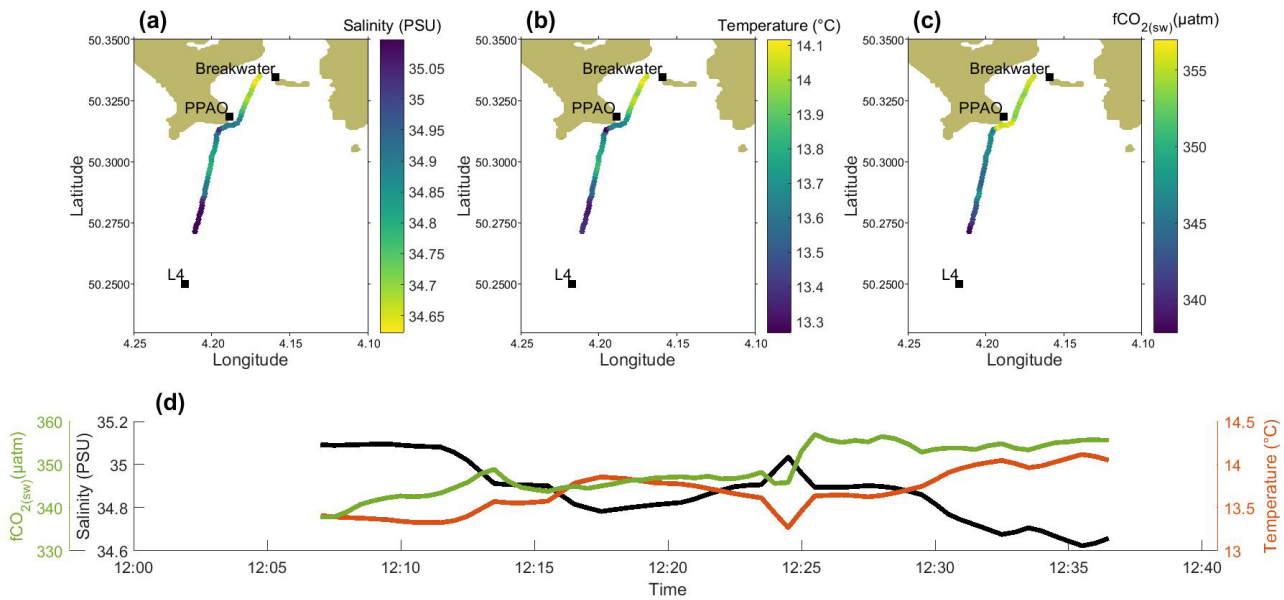


**Figure 5.** Example of a flooding tide transect (transect midpoint = LW + 3.5 h). Surface measurements of salinity, temperature and  $f\text{CO}_2$  represented spatially (a–c) and as a time series (d) from station L4 toward the coast. Data were collected aboard RV *Plymouth Quest* on 15 June 2016, (filled circles, data every 30 s).

Data collected on 30 June are an example of a transect at high water (LW + 6 h, Fig. 6). High-salinity (> 35) water was observed much closer to PPAO during the LW + 6 h transect than on transects during low water periods in the tidal cycle (Figs. 4 and 5). Salinity reduces rapidly to 34.1 in between the PPAO and the breakwater. Spatial patterns similar to surface salinity are seen in SST and  $f\text{CO}_2$ , with the gradients the

inverse of the salinity gradient. The low-salinity water close to the breakwater has higher SST and  $f\text{CO}_2$  (14.8 °C and 385  $\mu\text{atm}$ ) than the observations south of PPAO. The  $f\text{CO}_2$  range on this transect was ~ 38  $\mu\text{atm}$ , and the majority of the change was close to the PPAO. The  $f\text{CO}_2$  difference between L4 and the water just south of PPAO was only ~ 12  $\mu\text{atm}$ . These data suggest that the Tamar plume during LW + 6 h

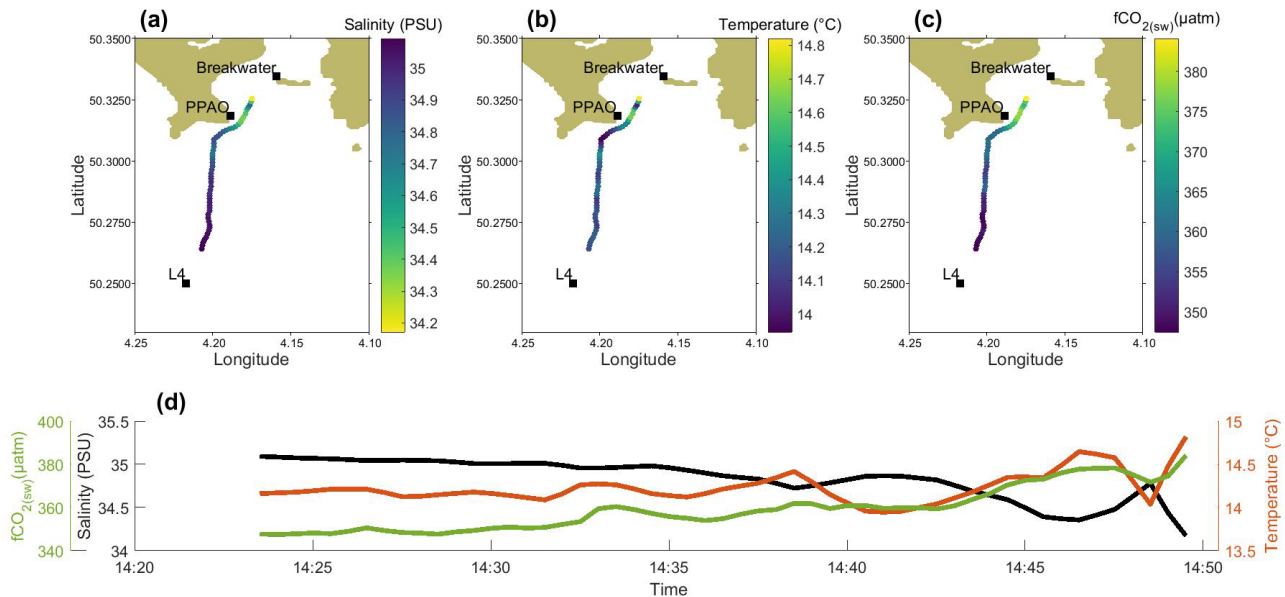


**Figure 6.** Example of a high water transect (transect midpoint = LW + 6 h). Surface measurements of salinity, temperature and  $f\text{CO}_2$  represented spatially (a–c) and as a time series (d) from station L4 toward the coast. Data were collected aboard RV *Plymouth Quest* on 30 June 2016, (filled circles, data every 30 s).

was restricted near to the coast and did not make a big impact upon the waters in between PPAO and L4.

Data on 10 June show a transect during an ebbing tide (LW + 9 h) (Fig. 7). Salinity near to L4 was 35.15 and declined toward the coast, interrupted by a patch of water due east of PPAO with salinity levels similar to L4. Two patches of low-salinity water (34.8) were encountered along the transect. One low-salinity patch was just south of PPAO and the other patch was close to the breakwater. Spatial variations in SST and  $f\text{CO}_2$  coincide with the variations in salinity, with higher SST ( $\sim 14.2^\circ\text{C}$ ) and  $f\text{CO}_2$  ( $\sim 365\ \mu\text{atm}$ ) in the patches of low-salinity water. The  $f\text{CO}_2$  difference between L4 surface waters and the fresh, warm waters influenced by the River Tamar plume is  $\sim 25\ \mu\text{atm}$ .

In summary, the variations in salinity observed in all transects (i.e. examples above and those in Fig. S2) qualitatively agreed with output from a previous physical model of the Plymouth Sound (Siddorn et al., 2003). The freshwater plume at low water extends out past the PPAO, whereas the plume at high water (LW + 6 h) is restricted to close to the breakwater (Siddorn et al., 2003). The same model on an ebbing tide predicts that two plumes of river water exit via the channels at the east and west ends of the breakwater.

### 3.4 Relationship between salinity and $f\text{CO}_2$

The changes in salinity and  $f\text{CO}_2$  during the example transects suggest that the changes in  $f\text{CO}_2$  are driven by conservative mixing of salt water and freshwater endmembers. Robust  $f\text{CO}_2$  and salinity relationships have been observed in large river plumes like the Amazon and Mississippi (Lefèvre

et al., 2010; Cai et al., 2013). The relationship between salinity and  $f\text{CO}_2$  is complicated by the seasonal variability in  $f\text{CO}_2$  and the constantly changing position of the tidally controlled freshwater plume. We calculated the difference between in situ data from transects and from measurements at L4 to account for seasonal variations in seawater  $\text{CO}_2$ :

$$\xi f\text{CO}_2 = \text{Transect}f\text{CO}_2 - \text{L4}f\text{CO}_2, \quad (4)$$

$$\xi S = \text{TransectSalinity} - \text{L4Salinity}. \quad (5)$$

$\xi f\text{CO}_2$  and  $\xi S$  displayed an apparent relationship throughout different seasons and stages of the tidal cycle (Fig. 8).  $\xi S$  was a stronger predictor of  $\xi f\text{CO}_2$  than location along the transect (distance from L4).

The  $f\text{CO}_2$  and salinity data diverged from the general trend when the RV *Plymouth Quest* travelled into Cawsand Bay (west of the breakwater) on 7 July (Fig. 8). Uncles and Torres (2013) showed that the seawater residence time increases as you approach the breakwater; following that methodology, the FVCOM model used here also shows this is true for Cawsand Bay. A long residence time and a shallow water column mean that the waters in Cawsand Bay are likely to be closer to equilibrium with the atmosphere due to relatively higher turbulent mixing from bottom stress and surface waves (Upstill-Goddard, 2006). As Cawsand Bay is a microscale environment ( $< 1\ \text{km}^2$ ), the bay could be a biological hotspot driving the changes in  $\text{CO}_2$ . Excluding the 7 July transect that went into Cawsand Bay, the linear fit to the  $\xi f\text{CO}_2$  and  $\xi S$  data gives  $\xi f\text{CO}_2 = -39.83 \xi S + 5.50$  ( $R^2 = 0.2165$ ,  $N = 22\,262$ ,  $p < 0.001$ ). The fit explained

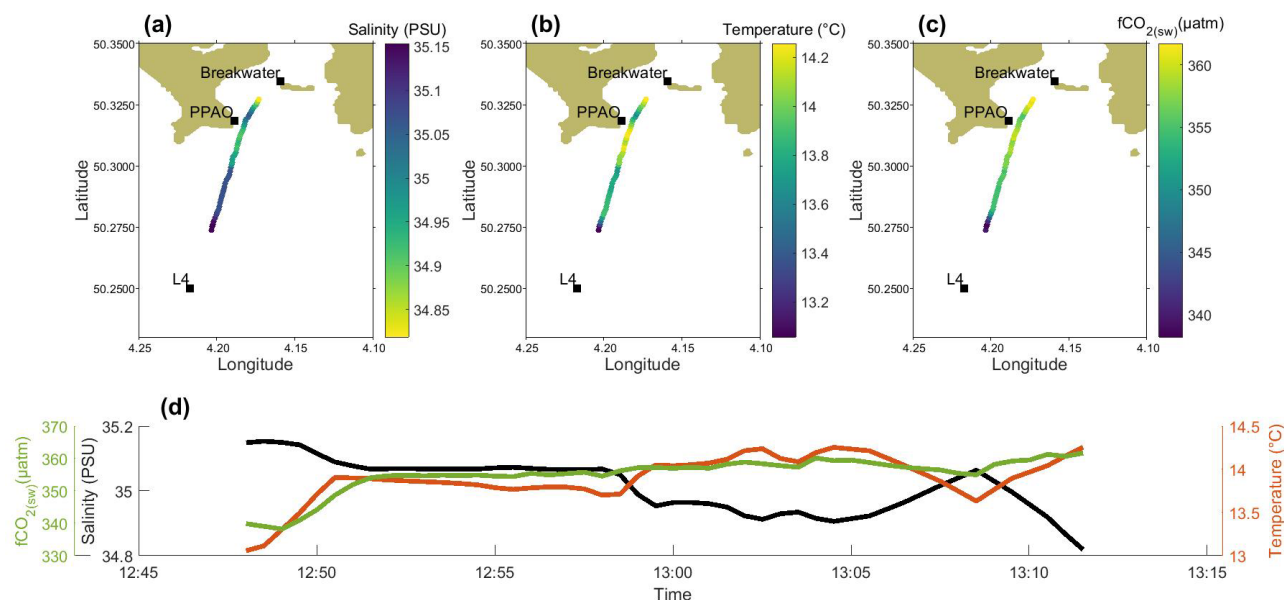


**Figure 7.** Example of an ebbing tide transect (transect midpoint = LW + 8.75 h). Surface measurements of salinity, temperature and  $f\text{CO}_2$  represented spatially (a–c) and as a time series (d) from station L4 toward the coast. Data were collected aboard RV *Plymouth Quest* on 10 June 2016, (filled circles, data every 30 s).

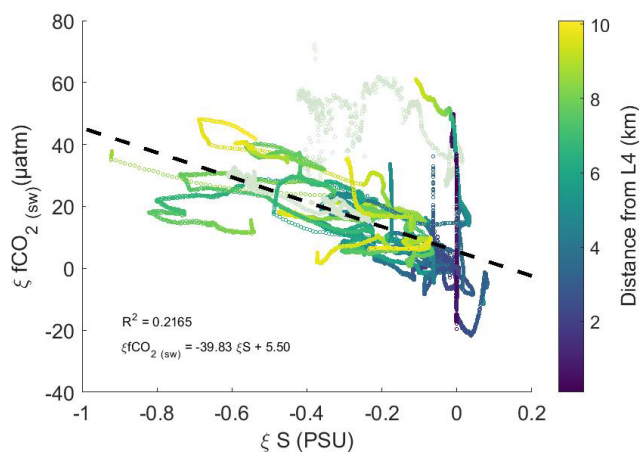


**Figure 8.** Scatter plot of  $\xi S$  versus  $\xi f\text{CO}_2$ ; difference of data from transects between Plymouth Breakwater and station L4 between 10 June and 21 September 2016. Data are coloured by their distance from station L4; the dashed black line is the best fit for the data. The data for 7 July are shown in light grey.

21.6% of the variability in the data, with a RMSE of 18.95  $\mu\text{atm}$ .

$f\text{CO}_2$  values calculated from TA and DIC bottle data from the River Tamar on 1 October 2014 show a qualitatively similar relationship between salinity and  $f\text{CO}_2$  (Fig. S5 in the Supplement) for stations T3–T9. The trend continues for stations furthest upstream (T1 and T2) but does not follow the same linear relationship. A linear fit between  $\xi S$  and  $\xi f\text{CO}_2$  for stations T3–T9 suggests a 42.24  $\mu\text{atm}$  change per unit of

salinity. The bottle data indicate that the  $\xi f\text{CO}_2$  and  $\xi S$  relationship can be extrapolated to lower salinities and that the relationship begins to break down at  $\xi S < -4$ . Note that the TA/DIC data and  $f\text{CO}_2$  data were collected at different times (years and stages of seasonal cycle) and with different sampling and analytical approaches. The apparent linear relationship between  $\xi f\text{CO}_2$  and  $\xi S$  suggested that it can be applied to the wider coastal region. The next section assesses the utility of the high-resolution model (Uncles et al., 2020) to predict coastal  $f\text{CO}_2$ .

### 3.5 Using FVCOM to estimate coastal air–sea $\text{CO}_2$ fluxes

Extrapolation of the relationship between  $\xi S$  and  $\xi f\text{CO}_2$  across the coastal domain required that FVCOM accurately replicates available surface salinity observations at different stages of the tidal cycle. FVCOM compares very well with the spatial and temporal variability in the four example transects at different stages of the tidal cycle (Fig. 9), even though the hourly resolution of the model means the model output frequency cannot capture subtle changes in frontal positions that are penalised in point-to-point comparisons. Model agreement with the  $\xi S$  observations ( $-0.1 > \xi S < 4$ ) from all 15 transects was also good (RMSE = 0.213), which indicates that FVCOM can be used as a reliable indication of spatial and temporal salinity changes during the observation period (June–September 2016) (Fig. S6 in the Supplement).

Modelled spatial variations in coastal surface salinity are shown in Fig. 10a, which focuses on the 7 July transect. Equivalent plots for the other three example transects on

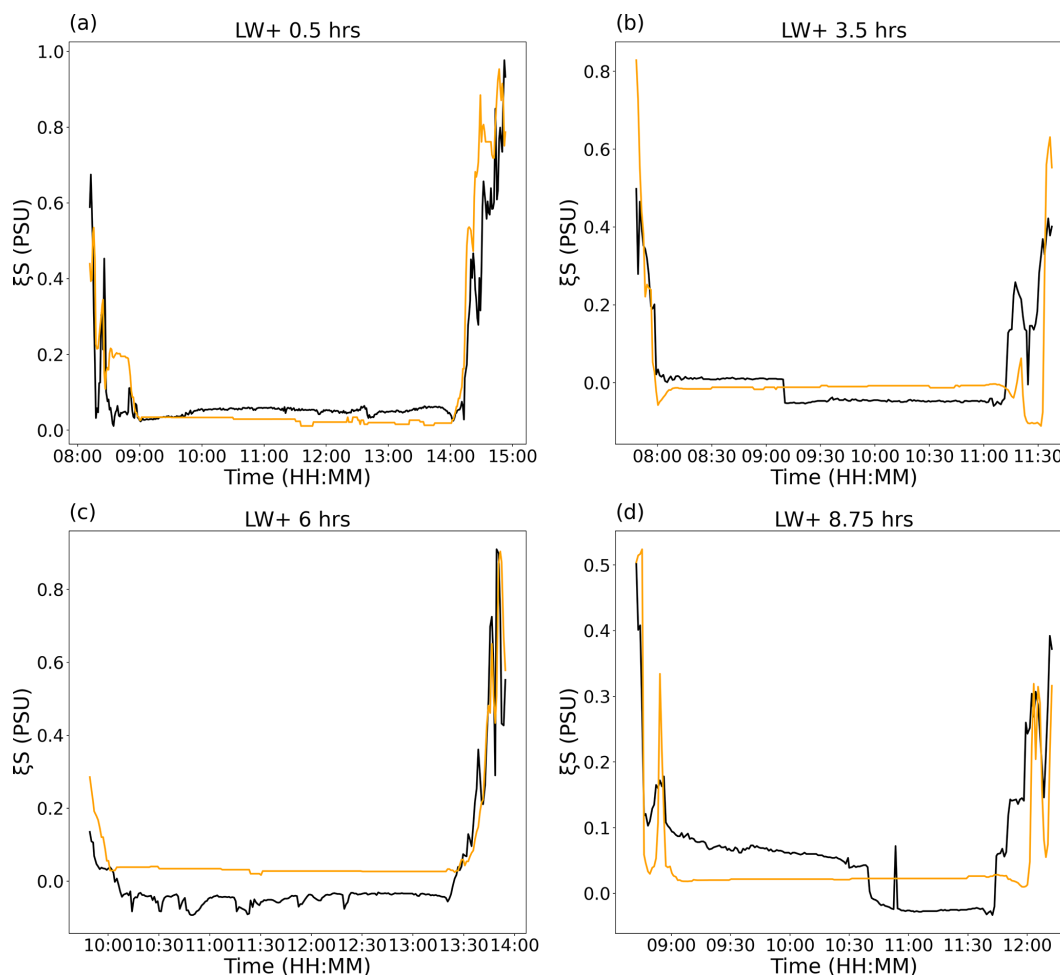


**Figure 9.** Comparison of  $\xi S$  from surface observations (underway RV *Plymouth Quest*, black) and the FVCOM model (orange). Each of the four panels corresponds to the four example transects from four stages of the tidal cycle: (a) 7 July (LW + 0 h), (b) 15 June (LW + 3.5 h), (c) 30 June (LW + 6 h) and (d) 10 June (LW + 8.75 h).

30 June, 15 June and 10 June (Figs. S7 to S9 in the Supplement). The 7 July transect was at low water (LW + 0 h) and when low-salinity water was exiting from either side of the breakwater and wrapping around the Rame Head peninsula (Fig. 10a).

FVCOM output was combined with surface measurements of  $f\text{CO}_2$  at L4 (Kitidis et al., 2012) to predict coastal variability in air–sea  $\text{CO}_2$  fluxes (Fig. 10b). The model domain for estimated  $f\text{CO}_2$  is restricted (i) to cover the region inshore of L4 ( $> 50.24^\circ \text{N}$ , Fig. 10b), (ii) to avoid regions where gas exchange is largely caused by bottom-driven turbulence (bottom depth  $> 10 \text{ m}$ ) and (iii) to avoid over-extrapolating the relationship observed in Fig. 8 ( $\xi S > -4$ , equivalent to a minimum salinity of approximately 30). The model domain excludes the upper sections of the rivers and the upper estuary and shallow coastal waters such as Cawsand Bay. The model results suggest that the majority of the coastal waters (Plymouth Sound and surroundings) contain  $f\text{CO}_2$  levels that

are substantially higher ( $> 100 \mu\text{atm}$ ) than L4 at this stage of the tidal cycle (low water, LW + 0 h).

The standard combined uncertainty for calculated  $f\text{CO}_2$  values is consistent with the International Bureau of Weights and Measures (BIPM) guide to the expression of uncertainty in measurement (GUM) methodology (JCGM, 2008). In determining  $\xi S$ , there is the uncertainty in modelled salinity ( $\text{Transect}_{\text{Salinity}}$ ) given as the RMSE of the model salinity (0.213) and the instrument uncertainty in the salinity at L4 ( $L4_{\text{Salinity}}$  for Wetlabs WQM = 0.003; Smyth et al., 2010a), which add in quadrature. The combined model and instrument  $\xi S$  uncertainty is propagated through the  $\xi/f\text{CO}_2$  and  $\xi S$  equation to give an uncertainty due to  $\xi S$  ( $8.48 \mu\text{atm}$ ). The standard combined uncertainty in  $f\text{CO}_2$  includes the uncertainty in the  $\xi/f\text{CO}_2$  and  $\xi S$  relationship ( $18.95 \mu\text{atm}$ ), uncertainty due to  $\xi S$  ( $8.48 \mu\text{atm}$ ), and the uncertainty in the  $f\text{CO}_2$  observations ( $L4 f\text{CO}_2 = 6.9 \mu\text{atm}$ , from the on station comparison, Fig. 2). These uncertainties add in quadrature to give a standard combined uncertainty of  $21.88 \mu\text{atm}$ .

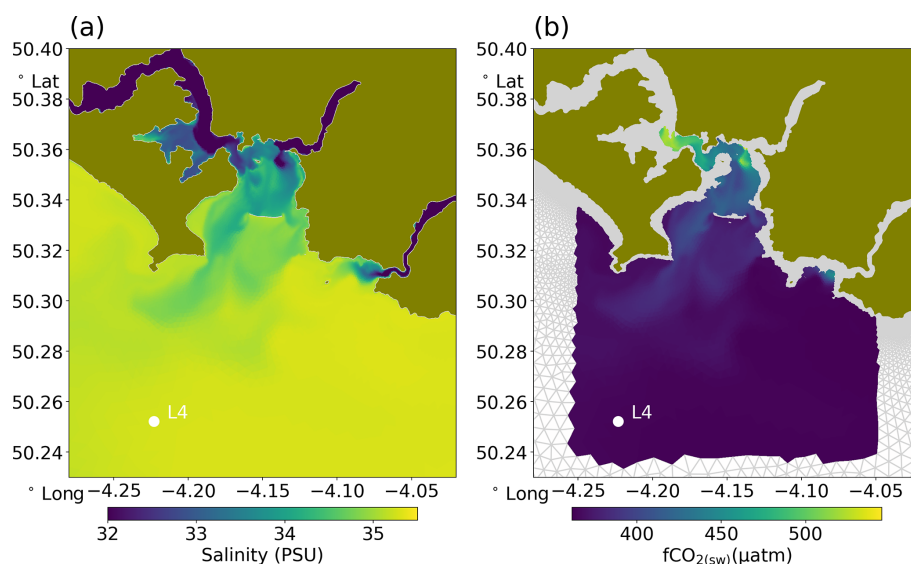


**Figure 10.** (a) Model surface salinity field on 7 July at the midpoint of the observational transect. Note that the range of the colour bar was restricted to better depict salinity in the lower estuary, and thus salinity in the upper estuaries is beyond the range of the colour bar. (b) Derived  $\xi f\text{CO}_2$  using the determined  $\xi S$  and  $\xi f\text{CO}_2$  relationship.

The FVCOM model enables simulation of a full tidal cycle so that the impact on air–sea  $\text{CO}_2$  flux can be visualised throughout 7 July (Fig. 11; equivalent figures for the examples on 30, 15 and 10 June are in Figs. S10 to S12 in the Supplement). A constant wind speed (equal to the mean during that period) is applied across the model domain (surface area =  $132 \text{ km}^2$ ) for simplicity. The flux signal co-varies with tidal height (Fig. 11a and b). The flux integrated across the model domain changes substantially throughout the tidal cycle ( $\sim 9\%$  change). If the region is restricted further to include just the area north of PPAO ( $> 50.32^\circ \text{ N}$ ), then the magnitude of the flux changes substantially from a weak sink ( $\sim -65 \text{ mol h}^{-1}$ ) at low tide to a substantially larger sink ( $\sim -1100 \text{ mol h}^{-1}$ ) at high tide.

Three configurations were used to calculate the flux (Fig. 12) to establish whether the tidal plume had a net effect on the regional air–sea fluxes calculated on seasonal timescales between March and November 2016. In the first configuration (L4), L4 measurements were extrapolated across the study area. The second configuration (this study) combined the L4 measurements with the  $f\text{CO}_2$  and salinity relationship (Fig. 8) and applied the result to the spatially varying salinity field from the FVCOM model. In the third configuration (Landschützer coastal product), the  $\text{CO}_2$  value from closest node ( $50.125^\circ \text{ N}$ ,  $4.125^\circ \text{ W}$ ) in the Landschützer coastal product (Landschützer et al., 2020) is extrapolated across the study area. Fluxes were computed for a fixed region of  $128 \text{ km}^2$  (a slight modification of the region in Figs. 10b and 11a–d) encompassing the river plume and the region behind the breakwater. Areas that met the depth and salinity criteria in the region (depth  $> 10 \text{ m}$ ,  $\xi S > -4$  and  $> 50.24^\circ \text{ N}$ ) for  $> 80\%$  of the period were included.

Whilst  $f\text{CO}_2$  is typically measured weekly at L4 by the showerhead system, instrument downtime in 2016 meant that the measurements were less frequent than normal, leading to interpolation between measurements to construct a non-fragmented time series of seasonal  $f\text{CO}_2$  in 2016 (an unavoidable limitation of this approach). The average regional  $f\text{CO}_2$  (i.e. including using the spatially varying salinity) showed undersaturation in the summer and oversaturation in the spring and autumn. The regional concentration was  $\sim 30 \mu\text{atm}$  greater than the observed concentrations at L4, which is larger than the uncertainty in our estimate of  $f\text{CO}_2$  (Fig. 12). The  $p\text{CO}_2$  in the Landschützer coastal product was much lower than the observed  $f\text{CO}_2$  values at L4 in 2016 (Fig. 12).

L4  $p\text{CO}_2$  saturations (Fig. 12) indicate that fluxes follow the same trend as previous measurements at the site:  $\text{CO}_2$  uptake in the region throughout the summer and a short period of outgassing in late September (Kitidis et al., 2012; Marrec et al., 2013). The Landschützer product suggests that the region is a larger sink than indicated by the measurements at L4 and does not indicate that the region is ever a source of  $\text{CO}_2$  to the atmosphere. This study calculates fluxes using  $f\text{CO}_2$  values predicted from salinity and suggests that the near-coastal region ( $128 \text{ km}^2$ ) was a weaker sink in summer, increasing the discrepancy with the Landschützer product. This study also suggests weak outgassing of  $\text{CO}_2$  near the coast in March, April and October

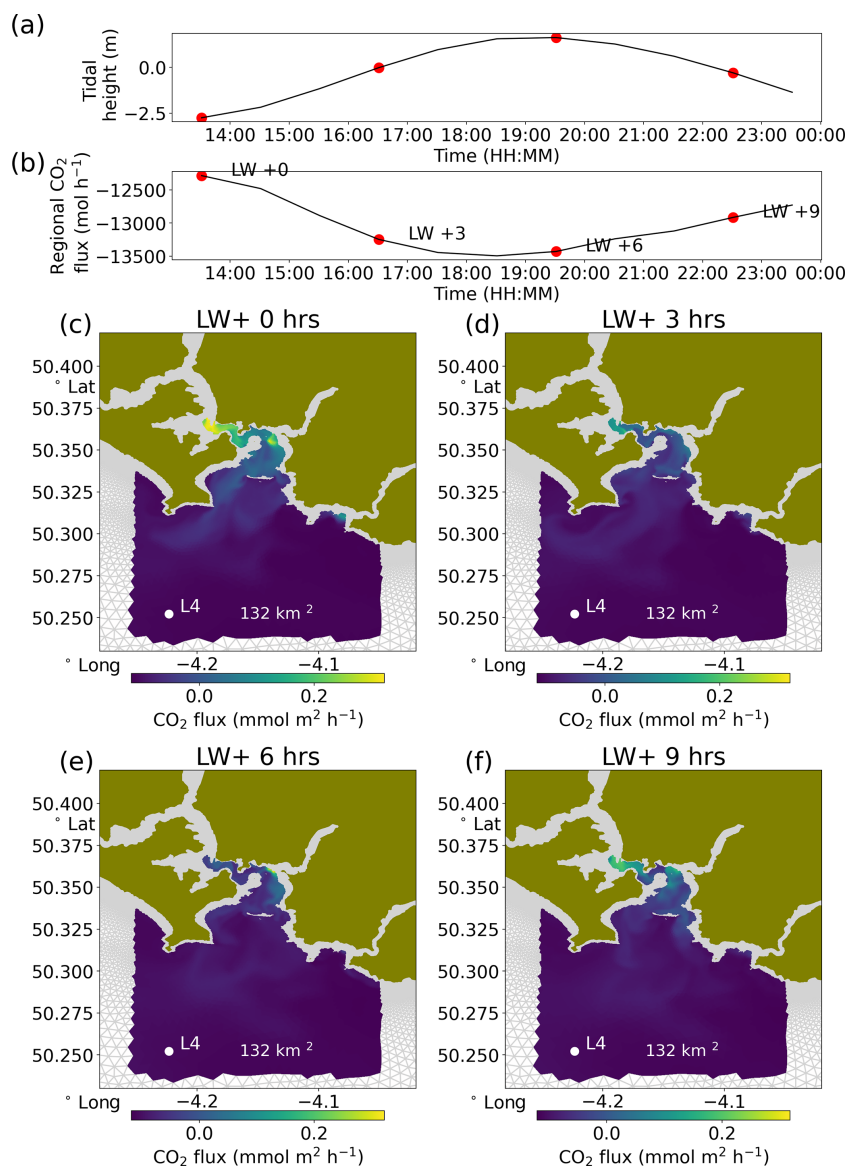


**Figure 11.** Modelled impact of a full tidal cycle (a) on tidal height and (b) on air–sea  $\text{CO}_2$  flux in the coastal zone (hourly calculations; negative fluxes are into the ocean) on 7 July 2016 with a fixed wind speed of  $5.3 \text{ m s}^{-1}$ . The total integrated air–sea  $\text{CO}_2$  flux within the modelled domain (c–f). Spatial variation in flux at four different stages of the 12 h tidal cycle is shown: LW + 0 h (c), LW + 3 h (d), LW + 6 h (e) and LW + 9 h (f). The red dots in panels (a) and (b) correspond to panels (c)–(f).

#### 4 Discussion

Here we show large variations in  $f\text{CO}_2$  in the estuarine zone using a high-frequency membrane equilibrator which could not be detected using a showerhead equilibrator. Seawater  $f\text{CO}_2$  is assumed to be relatively homogeneous over large spatial scales in the open ocean (Takahashi et al., 2009). Temporal variability in open-ocean waters is also typically slow, with the most rapid variations occurring over hourly or slower timescales (e.g. diurnal Torres et al., 2021). The measuring frequency of a typical showerhead seawater  $\text{CO}_2$  system ( $\sim 8 \text{ min}$ ) is thus sufficient to determine open-

ocean  $f\text{CO}_2$  variability. The difference between the underway  $f\text{CO}_2$  measurements made by the two systems used in this study (Fig. 2) is caused by the different response times of the showerhead and membrane equilibrators and their ability to resolve the considerable horizontal variability in coastal and shelf waters (Kitidis et al., 2012). The membrane and showerhead systems agreed well when the ship was on station ( $\text{RMSE} = 6.9 \mu\text{atm}$ ), because both systems had sufficient time to equilibrate. When the ship was moving through heterogeneous coastal surface waters, the showerhead system cannot fully equilibrate, and the agree-

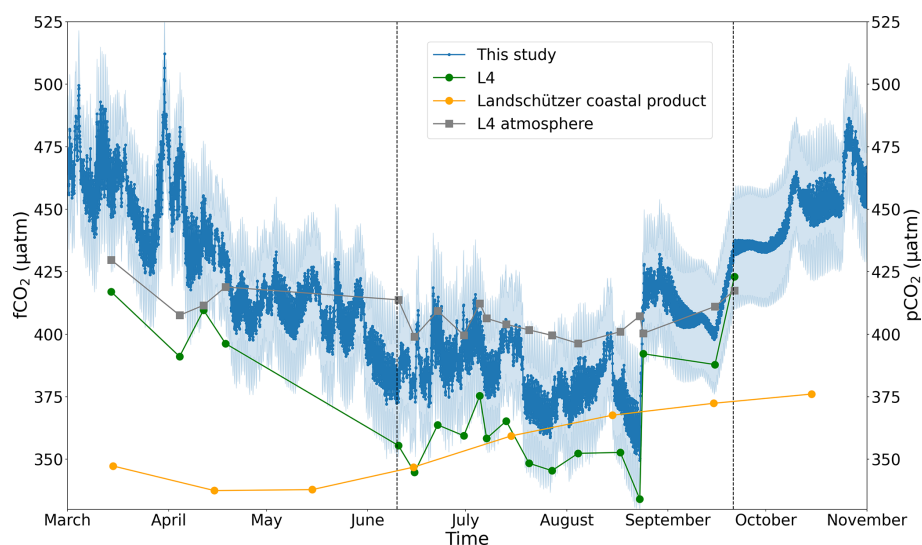


**Figure 12.**  $f\text{CO}_2$  and  $p\text{CO}_2$  values used to calculate the regional  $\text{CO}_2$  flux over the domain ( $128 \text{ km}^2$ , approximately same as in above figures). Measurements of  $f\text{CO}_2$  made by RV *Plymouth Quest* on station at L4 (L4, green dots).  $p\text{CO}_{2(\text{atm})}$  measured by RV *Plymouth Quest* on station at L4 (grey squares). The results of this study; hourly average  $f\text{CO}_2$  across the valid model domain used for long-term flux calculations (this study, blue dots). The standard combined uncertainty in the data from this study is indicated by the shaded background in light blue. The monthly Landschützer  $p\text{CO}_2$  data (Landschützer coastal product, orange dots) are from the closest valid node ( $50.125^\circ \text{ N}$ ,  $4.125^\circ \text{ W}$ ) in the Landschützer et al. (2020) coastal data product. It is noted that the Landschützer node is outside of the model domain (which has a lower boundary of  $50.24^\circ \text{ N}$ ). The vertical dashed lines indicate the dates of the first and last measurement transects.

ment with the fast-response membrane equilibrators system is worse ( $\text{RMSE} = 27.1 \mu\text{atm}$ ).

Single seawater  $\text{CO}_2$  observations are representative of  $\text{CO}_2$  integrated across the region that the ship transits through whilst equilibrating. The RV *Plymouth Quest* typically travels at  $\sim 9$  knots ( $4.6 \text{ m/s}$ ), which is equivalent to  $0.22 \text{ km}$  in  $48 \text{ s}$  (two  $e$ -folding times response time of the membrane system) and  $1.1 \text{ km}$  in  $4 \text{ min}$  (two  $e$ -folding times response time of the showerhead system). However, the showerhead system also switches between seawater  $\text{CO}_2$ ,  $\text{CO}_2$  gas standards and atmospheric  $\text{CO}_2$ ; hence, seawater  $f\text{CO}_2$  measurements are  $27 \text{ min}$  apart, which equates to a distance of  $\sim 7.5 \text{ km}$  when the RV *Plymouth Quest* is moving.

We identified an inverse linear relationship between salinity and  $f\text{CO}_2$  and that salinity measurements also agreed well with model salinity output. The FVCOM model output confirms that the river plume extent is highly variable in time and space and that oceanographic features in the region such as the river plume are  $\sim 1 \text{ km}$  or smaller. The highly dynamic nature of the plume means that a showerhead  $\text{CO}_2$  system cannot be expected to resolve the spatial dynamics. A showerhead  $f\text{CO}_2$  system design can also be biased toward the end of the equilibration period, which may generate some measurement bias if seawater  $f\text{CO}_2$  changes rapidly during the  $8 \text{ min}$  full equilibration time (e.g. Ribas-Ribas et al., 2014). Complete characterisation of  $f\text{CO}_2$  in coastal waters within  $10 \text{ km}$  of land and with highly variable  $f\text{CO}_2$  requires a system with a fast-response equilibrator or slower steaming.

Mixing of estuarine and continental shelf water masses partially determines the  $f\text{CO}_2$  levels observed in this nearshore study region. Shelf waters exhibit a seasonal surface  $f\text{CO}_2$  trend associated with (a) cooling-enhanced solubility in late winter, (b) net phytoplankton uptake in spring/summer, (c) partial re-equilibration with the atmosphere and (d) mixing with  $\text{CO}_2$ -rich bottom waters in autumn (Kitidis et al., 2019). The River Tamar is the other mixing endmember and is typically oversaturated with  $f\text{CO}_2$  with respect to the atmosphere (Frankignoulle et al., 1998). The results presented in this paper also suggest that riverine  $f\text{CO}_2$  may have a strong influence on the spatial and temporal patterns in coastal waters off Plymouth. It is important to note that the relationship between salinity and  $f\text{CO}_2$  determined in this paper only explains  $21.6 \%$  of the variability and was derived with summer data only (due to sampling constraints). Further work is needed to confirm if the relationship holds during the remaining period of the year (i.e. October through to May).

The  $f\text{CO}_2$  variability that is not explained by our relationship could be driven by other factors. Close to the coast such as in Cawsand Bay, these include gas exchange in shallow waters, changes in  $\text{CO}_2$  concentration in the river, excess river runoff during storms,  $\text{CO}_2$  production in sediments, upwelling of water with different  $\text{CO}_2$  concentration and biological activity stimulated by nutrients in the Tamar plume. Biological processes in coastal ecosystems can strongly influence seawater  $\text{CO}_2$  levels (Cai et al., 2020), which may explain some of the large  $\text{CO}_2$  changes observed around L4

that are not linked to salinity changes.  $f\text{CO}_2$  changes due to photosynthesis are typically a few micro-atmospheres per day (Kitidis et al., 2019), so large differences will likely have built up over time. Water masses with  $f\text{CO}_2$  levels different to L4 may well be caused by factors such as biological activity and then the water advected toward L4 by currents.

The confluence of estuarine and continental shelf waters near the PPAO/breakwater and the local circulation of surface waters are dominated by the semi-diurnal tidal cycle (Uncles et al., 2015). The rising tide after low water pushes shelf water toward the breakwater, whereas a falling tide after high water encourages riverine-influenced water to extend south. The tidal influence upon coastal  $f\text{CO}_2$  is evident in the 15 transects during this study, with changes of 20–40  $\mu\text{atm}$  relative to L4 (Fig. 8). Time series data presented by Borges and Frankignoulle (1999) indicate a similar magnitude (20–25  $\mu\text{atm}$ ) tidal signature in coastal Belgian and Dutch waters.

The salinity field from the FVCOM model is used to estimate the surface  $f\text{CO}_2$  features over a complete tidal cycle and shows that the flux can change by a non-trivial amount ( $\sim 9\%$ ) over a short period of time (Fig. 11). These data also show that using a hydrodynamic model can extend the spatial and temporal coverage of  $\text{CO}_2$  uptake and outgassing estimates in the coastal region surrounding Plymouth made with weekly L4 measurements (Fig. 12). If similar relationships can be developed for other estuarine zones, then operational dynamic models may also be able to add information to flux estimates for these zones. The spatial resolution of the model at the surface means that it is possible that near-surface features such as freshwater lenses are overlooked by this analysis. Higher-resolution modelling of the surface ocean would make future coastal products more applicable to air–sea flux studies.

## 5 Conclusions

Here we show for the first time dynamic and large variations in the coastal zone using a fast-response membrane equilibrator system. These gradients between estuarine waters and shelf waters were not resolved by a co-located showerhead  $\text{CO}_2$  system. The gradients in salinity and  $f\text{CO}_2$  fields show strong tidal influence. Changes in  $f\text{CO}_2$  after accounting for the seasonal trend are linked with salinity variations, with the highest regions of  $f\text{CO}_2$  coinciding with the lowest salinity regions and vice versa. The inverse linear relationship between salinity and  $f\text{CO}_2$  variations (Fig. 8) suggests that mixing of estuarine and shelf water endmembers is a control on the surface water distribution of  $f\text{CO}_2$ . Measured salinity agrees well with FVCOM model surface salinity fields at different stages of the tidal cycle. FVCOM output is used to estimate the temporal and spatial variations of  $f\text{CO}_2$  in coastal waters. The model output demonstrates that neglecting the river plume leads to an overestimation of the magnitude of the  $\text{CO}_2$  sink in the summer. The region may also

be misidentified as a sink for atmospheric  $\text{CO}_2$  in the spring and autumn when it could be a weak source, as suggested by Torres et al. (2020). Measurements from L4 are not representative of the estuarine zone, and caution should be used when scaling them over this region.

The surface flux from estuaries and coastal waters has proven difficult to assess comprehensively (Borges et al., 2006). The high-resolution  $f\text{CO}_2$  data presented in this study show that tidal and estuarine-influenced coastal waters can quickly transition from a strong source to a strong sink depending on the state of the tide (Fig. 11). Inland and coastal waters are a large uncertainty in global fluxes (Chen et al., 2013). The high-resolution observations presented in this paper show that the head of the river/estuarine plume for this region is linked to the tidal state. This is critical for the accurate calculation of air–water flux from the region. Further studies are required to evaluate the wider applicability of this method to similar coastal regions. Distinctly different estuarine/coastal zones such as lagoons, river deltas and fjords will have their own distinct  $f\text{CO}_2$  signatures and patterns driven in part by surface water circulation and mixing. High-resolution models that can resolve tides and surface salinity in estuarine/coastal waters with high confidence are a useful tool in ongoing and future efforts to constrain coastal air–sea  $\text{CO}_2$  fluxes.

*Code availability.* The MATLAB and Python scripts used during this analysis are provided in the Supplement and are also hosted at <https://doi.org/10.5281/zenodo.6373406> (Sims, 2022).

*Data availability.* The high-frequency  $p\text{CO}_2$  data, the river transect bottle data and the RV *Plymouth Quest* underway  $p\text{CO}_2$  data used in this paper are available in the Supplement. The FVCOM model data output is available at <https://doi.org/10.5281/zenodo.6372107> (Bedington and Torres, 2022).

*Supplement.* The supplement related to this article is available online at: <https://doi.org/10.5194/bg-19-1657-2022-supplement>.

*Author contributions.* RPS wrote the manuscript with assistance from all co-authors. RPS made the high-frequency  $p\text{CO}_2$  measurements on RV *Plymouth Quest*. RPS completed the analysis and interpretation of the data with support from TGB, US and AJW. MB with support from RT ran the FVCOM model and helped with interpreting the model output. VK helped with the interpretation of the RV *Plymouth Quest*  $p\text{CO}_2$  data; IB maintained the  $p\text{CO}_2$  instrumentation on RV *Plymouth Quest*. JRF helped with interpretation of the RV *Plymouth Quest* underway data and maintained this instrumentation. HSF analysed the TA and DIC data collected during the river transect on *PML Explorer*.

*Competing interests.* The contact author has declared that neither they nor their co-authors have any competing interests.

*Disclaimer.* Publisher's note: Copernicus Publications remains neutral with regard to jurisdictional claims in published maps and institutional affiliations.

*Acknowledgements.* We thank the captain and crew of the RV *Plymouth Quest* for all their assistance. We also thank Tim Smyth and Ming Yang for insightful discussions and data relating to the WCO and PPAO time series and John Stevens and Rachel Beale for their help on the *PML Explorer*.

*Financial support.* This research was supported by UK NERC (studentship NE/L000075/1), the Shelf Sea Biogeochemistry pelagic research programme (NE/K002007/1), RAGNARoCC (NE/K002473/1), Climate Linked Atlantic Sector Science (CLASS; NE/R015953/1), the Land Ocean Carbon Transfer project (LO-CATE; NE/N018087/1), NERC grant NE/L007010 and the NERC LTSS national capability programme that underpins numerical modelling work at PML. This research was also supported by EU projects MyCOAST (EU Interreg Atlantic Area programme project MyCOAST, EAPA\_285/2016), IMMERSE (H2020 821926), AtlantOS (H2020 633211), FixO3 (FP7 312463) and RINGO (H2020 730944).

*Review statement.* This paper was edited by Jack Middelburg and reviewed by Wei-Jun Cai and two anonymous referees.

## References

- Abril, G., Bouillon, S., Darchambeau, F., Teodoru, C. R., Marwick, T. R., Tamooh, F., Ochieng Omengo, F., Geeraert, N., Deirmendjian, L., Polsenaere, P., and Borges, A. V.: Technical Note: Large overestimation of  $p\text{CO}_2$  calculated from pH and alkalinity in acidic, organic-rich freshwaters, *Biogeosciences*, 12, 67–78, <https://doi.org/10.5194/bg-12-67-2015>, 2015.
- Ahmed, M. and Else, B. G.: The Ocean  $\text{CO}_2$  Sink in the Canadian Arctic Archipelago: A Present-Day Budget and Past Trends Due to Climate Change, *Geophys. Res. Lett.*, 46, 9777–9785, 2019.
- Bakker, D. C., de Baar, H. J., and de Wilde, H. P.: Dissolved carbon dioxide in Dutch coastal waters, *Mar. Chem.*, 55, 247–263, 1996.
- Bakker, D. C. E., Pfeil, B., Landa, C. S., Metzl, N., O'Brien, K. M., Olsen, A., Smith, K., Cosca, C., Harasawa, S., Jones, S. D., Nakaoka, S., Nojiri, Y., Schuster, U., Steinhoff, T., Sweeney, C., Takahashi, T., Tilbrook, B., Wada, C., Wanninkhof, R., Alin, S. R., Balestrini, C. F., Barbero, L., Bates, N. R., Bianchi, A. A., Bonou, F., Boutin, J., Bozec, Y., Burger, E. F., Cai, W.-J., Castle, R. D., Chen, L., Chierici, M., Currie, K., Evans, W., Featherstone, C., Feely, R. A., Fransson, A., Goyet, C., Greenwood, N., Gregor, L., Hankin, S., Hardman-Mountford, N. J., Harlay, J., Hauck, J., Hoppema, M., Humphreys, M. P., Hunt, C. W., Huss, B., Ibáñez, J. S. P., Johannessen, T., Keeling, R., Kitidis, V., Körtzinger, A., Kozyr, A., Krasakopoulou, E., Kuwata, A., Landshützer, P., Lauvset, S. K., Lefèvre, N., Lo Monaco, C., Manke, A., Mathis, J. T., Merlivat, L., Millero, F. J., Monteiro, P. M. S., Munro, D. R., Murata, A., Newberger, T., Omar, A. M., Ono, T., Paterson, K., Pearce, D., Pierrot, D., Robbins, L. L., Saito, S., Salisbury, J., Schlitzer, R., Schneider, B., Schweitzer, R., Sieger, R., Skjelvan, I., Sullivan, K. F., Sutherland, S. C., Sutton, A. J., Tadokoro, K., Telszewski, M., Tuma, M., van Heuven, S. M. A. C., Vandemark, D., Ward, B., Watson, A. J., and Xu, S.: A multi-decade record of high-quality  $f\text{CO}_2$  data in version 3 of the Surface Ocean  $\text{CO}_2$  Atlas (SOCAT), *Earth Syst. Sci. Data*, 8, 383–413, <https://doi.org/10.5194/essd-8-383-2016>, 2016.
- Bauer, J. E., Cai, W.-J., Raymond, P. A., Bianchi, T. S., Hopkinson, C. S., and Regnier, P. A.: The changing carbon cycle of the coastal ocean, *Nature*, 504, 61–70, <https://doi.org/10.1038/nature12857>, 2013.
- Bedington, M. and Torres, R.: Plymouth sound and surroundings surface temperature and salinity from FVCOM model, Zenodo [data set], <https://doi.org/10.5281/zenodo.6372107>, 2022.
- Borges, A. and Frankignoulle, M.: Daily and seasonal variations of the partial pressure of  $\text{CO}_2$  in surface seawater along Belgian and southern Dutch coastal areas, *J. Marine Syst.*, 19, 251–266, 1999.
- Borges, A., Schiettecatte, L.-S., Abril, G., Delille, B., and Gazeau, F.: Carbon dioxide in European coastal waters, *Estuar. Coast. Shelf S.*, 70, 375–387, 2006.
- Borges, A. V., Abril, G., and Bouillon, S.: Carbon dynamics and  $\text{CO}_2$  and  $\text{CH}_4$  outgassing in the Mekong delta, *Biogeosciences*, 15, 1093–1114, <https://doi.org/10.5194/bg-15-1093-2018>, 2018.
- Bozec, Y., Cariou, T., Macé, E., Morin, P., Thuillier, D., and Vernet, M.: Seasonal dynamics of air–sea  $\text{CO}_2$  fluxes in the inner and outer Loire estuary (NW Europe), *Estuar. Coast. Shelf S.*, 100, 58–71, 2012.
- Cai, W., Chen, C. A., and Borges, A.: Carbon dioxide dynamics and fluxes in coastal waters influenced by river plumes, in: *Biogeochemical Dynamics at Major River-Coastal Interfaces*, edited by: Bianchi, T. S., Allison, M. A., and Cai, W.-J., Cambridge University Press, Cambridge, 155–173, 2013.
- Cai, W.-J.: Estuarine and coastal ocean carbon paradox:  $\text{CO}_2$  sinks or sites of terrestrial carbon incineration?, *Annu. Rev. Mar. Sci.*, 3, 123–145, 2011.
- Cai, W.-J., Xu, Y.-Y., Feely, R. A., Wanninkhof, R., Jönsson, B., Alin, S. R., Barbero, L., Cross, J. N., Azetsu-Scott, K., and Fassbender, A. J.: Controls on surface water carbonate chemistry along North American ocean margins, *Nat. Commun.*, 11, 1–13, 2020.
- Cai, W.-J., Feely, R. A., Testa, J. M., Li, M., Evans, W., Alin, S. R., Xu, Y.-Y., Pelletier, G., Ahmed, A., and Greeley, D. J.: Natural and anthropogenic drivers of acidification in large estuaries, *Annu. Rev. Mar. Sci.*, 13, 23–55, 2021.
- Call, M., Maher, D. T., Santos, I. R., Ruiz-Halpern, S., Mangion, P., Sanders, C. J., Erler, D. V., Oakes, J. M., Rosentreter, J., and Murray, R.: Spatial and temporal variability of carbon dioxide and methane fluxes over semi-diurnal and spring–neap–spring timescales in a mangrove creek, *Geochim. Cosmochim. Ac.*, 150, 211–225, 2015.
- Canning, A. R., Fietzek, P., Rehder, G., and Körtzinger, A.: Technical note: Seamless gas measurements across the land–ocean aquatic continuum – corrections and evaluation of sensor data for  $\text{CO}_2$ ,  $\text{CH}_4$  and  $\text{O}_2$  from field deployments

- in contrasting environments, *Biogeosciences*, 18, 1351–1373, <https://doi.org/10.5194/bg-18-1351-2021>, 2021.
- Cazenave, P. W., Torres, R., and Allen, J. I.: Unstructured grid modelling of offshore wind farm impacts on seasonally stratified shelf seas, *Prog. Oceanogr.*, 145, 25–41, 2016.
- Chen, C., Liu, H., and Beardsley, R. C.: An unstructured grid, finite-volume, three-dimensional, primitive equations ocean model: application to coastal ocean and estuaries, *J. Atmos. Ocean. Tech.*, 20, 159–186, 2003.
- Chen, C.-T. A. and Borges, A. V.: Reconciling opposing views on carbon cycling in the coastal ocean: Continental shelves as sinks and near-shore ecosystems as sources of atmospheric CO<sub>2</sub>, *Deep-Sea Res. Pt. II*, 56, 578–590, 2009.
- Chen, C.-T. A., Huang, T.-H., Chen, Y.-C., Bai, Y., He, X., and Kang, Y.: Air–sea exchanges of CO<sub>2</sub> in the world’s coastal seas, *Biogeosciences*, 10, 6509–6544, <https://doi.org/10.5194/bg-10-6509-2013>, 2013.
- Dai, M., Lu, Z., Zhai, W., Chen, B., Cao, Z., Zhou, K., Cai, W. J., and Chenc, C. T. A.: Diurnal variations of surface seawater pCO<sub>2</sub> in contrasting coastal environments, *Limnol. Oceanogr.*, 54, 735–745, 2009.
- Dickson, A. G.: Standard potential of the reaction: AgCl(s) + 12 H<sub>2</sub>(g) = Ag(s) + HCl(aq), and the standard acidity constant of the ion HSO<sub>4</sub><sup>-</sup> in synthetic sea water from 273.15 to 318.15 K, *J. Chem. Thermodyn.*, 22, 113–127, 1990.
- Dickson, A. G. and Millero, F. J.: A comparison of the equilibrium constants for the dissociation of carbonic acid in seawater media, *Deep-Sea Res.*, 34, 1733–1743, 1987.
- Dickson, A. G., Sabine, C. L., and Christian, J. R.: Guide to best practices for ocean CO<sub>2</sub> measurements, Sidney, British Columbia, North Pacific Marine Science Organization, PICES Special Publication, 3, 176 pp., 2007.
- Fennel, K., Alin, S., Barbero, L., Evans, W., Bourgeois, T., Cooley, S., Dunne, J., Feely, R. A., Hernandez-Ayon, J. M., Hu, X., Lohrenz, S., Muller-Karger, F., Najjar, R., Robbins, L., Shadwick, E., Siedlecki, S., Steiner, N., Sutton, A., Turk, D., Vlahos, P., and Wang, Z. A.: Carbon cycling in the North American coastal ocean: a synthesis, *Biogeosciences*, 16, 1281–1304, <https://doi.org/10.5194/bg-16-1281-2019>, 2019.
- Ferrón, S., Ortega, T., Gómez-Parra, A., and Forja, J.: Seasonal study of dissolved CH<sub>4</sub>, CO<sub>2</sub> and N<sub>2</sub>O in a shallow tidal system of the bay of Cádiz (SW Spain), *J. Marine Syst.*, 66, 244–257, 2007.
- Frankignoulle, M., Bourge, I., Canon, C., and Dauby, P.: Distribution of surface seawater partial CO<sub>2</sub> pressure in the English Channel and in the Southern Bight of the North Sea, *Cont. Shelf Res.*, 16, 381–395, 1996.
- Frankignoulle, M., Abril, G., Borges, A., Bourge, I., Canon, C., Delille, B., Libert, E., and Théate, J.-M.: Carbon dioxide emission from European estuaries, *Science*, 282, 434–436, 1998.
- Friedlingstein, P., Jones, M. W., O’Sullivan, M., Andrew, R. M., Hauck, J., Peters, G. P., Peters, W., Pongratz, J., Sitch, S., Le Quéré, C., Bakker, D. C. E., Canadell, J. G., Ciais, P., Jackson, R. B., Anthoni, P., Barbero, L., Bastos, A., Bastrikov, V., Becker, M., Bopp, L., Buitenhuis, E., Chandra, N., Chevallier, F., Chini, L. P., Currie, K. I., Feely, R. A., Gehlen, M., Gilfillan, D., Gkritzalis, T., Goll, D. S., Gruber, N., Gutekunst, S., Harris, I., Haverd, V., Houghton, R. A., Hurtt, G., Ilyina, T., Jain, A. K., Joetzer, E., Kaplan, J. O., Kato, E., Klein Goldewijk, K., Korsbakken, J. I., Landschützer, P., Lauvset, S. K., Lefèvre, N., Lenton, A., Lienert, S., Lombardozzi, D., Marland, G., McGuire, P. C., Melton, J. R., Metz, N., Munro, D. R., Nabel, J. E. M. S., Nakaoka, S.-I., Neill, C., Omar, A. M., Ono, T., Peregon, A., Pierrot, D., Poulter, B., Rehder, G., Resplandy, L., Robertson, E., Rödenbeck, C., Séférian, R., Schwinger, J., Smith, N., Tans, P. P., Tian, H., Tilbrook, B., Tubiello, F. N., van der Werf, G. R., Wiltshire, A. J., and Zaehle, S.: Global Carbon Budget 2019, *Earth Syst. Sci. Data*, 11, 1783–1838, <https://doi.org/10.5194/essd-11-1783-2019>, 2019.
- Hales, B., Chipman, D., and Takahashi, T.: High-frequency measurement of partial pressure and total concentration of carbon dioxide in seawater using microporous hydrophobic membrane contractors, *Limnol. Oceanogr.-Meth.*, 2, 356–364, 2004.
- Hales, B., Takahashi, T., and Bandstra, L.: Atmospheric CO<sub>2</sub> uptake by a coastal upwelling system, *Global Biogeochem. Cy.*, 19, GB1009, <https://doi.org/10.1029/2004GB002295>, 2005.
- Haney, R. L.: On the pressure gradient force over steep topography in sigma coordinate ocean models, *J. Phys. Oceanogr.*, 21, 610–619, 1991.
- JCGM: Evaluation of measurement data – Guide to the expression of uncertainty in measurement, *Int. Organ. Stand. Geneva ISBN, Joint Committee for Guides in Metrology*, 50, 134, 2008.
- Jeffrey, L. C., Maher, D. T., Santos, I. R., Call, M., Reading, M. J., Holloway, C., and Tait, D. R.: The spatial and temporal drivers of pCO<sub>2</sub>, pCH<sub>4</sub> and gas transfer velocity within a subtropical estuary, *Estuar. Coast. Shelf S.*, 208, 83–95, 2018a.
- Jeffrey, L. C., Santos, I. R., Tait, D. R., Makings, U., and Maher, D. T.: Seasonal drivers of carbon dioxide dynamics in a hydrologically modified subtropical tidal river and estuary (Caboolture River, Australia), *J. Geophys. Res.-Biogeo.*, 123, 1827–1849, 2018b.
- Jiang, L. Q., Cai, W. J., Wanninkhof, R., Wang, Y., and Lüger, H.: Air–sea CO<sub>2</sub> fluxes on the US South Atlantic Bight: Spatial and seasonal variability, *J. Geophys. Res.-Oceans*, 113, C07019, <https://doi.org/10.1029/2007JC004366>, 2008.
- Joesoef, A., Huang, W.-J., Gao, Y., and Cai, W.-J.: Air–water fluxes and sources of carbon dioxide in the Delaware Estuary: spatial and seasonal variability, *Biogeosciences*, 12, 6085–6101, <https://doi.org/10.5194/bg-12-6085-2015>, 2015.
- Kahl, L. C., Bianchi, A. A., Osiroff, A. P., Pino, D. R., and Piola, A. R.: Distribution of sea-air CO<sub>2</sub> fluxes in the Patagonian Sea: Seasonal, biological and thermal effects, *Cont. Shelf Res.*, 143, 18–28, 2017.
- Kitidis, V., Hardman-Mountford, N. J., Litt, E., Brown, I., Cummings, D., Hartman, S., Hydes, D., Fishwick, J. R., Harris, C., and Martinez-Vicente, V.: Seasonal dynamics of the carbonate system in the Western English Channel, *Cont. Shelf Res.*, 42, 30–40, 2012.
- Kitidis, V., Brown, I., Hardman-Mountford, N., and Lefèvre, N.: Surface ocean carbon dioxide during the Atlantic Meridional Transect (1995–2013); evidence of ocean acidification, *Prog. Oceanogr.*, 158, 65–75, 2017.
- Kitidis, V., Shutler, J. D., Ashton, I., Warren, M., Brown, I., Findlay, H., Hartman, S. E., Sanders, R., Humphreys, M., and Kivimäe, C.: Winter weather controls net influx of atmospheric CO<sub>2</sub> on the north-west European shelf, *Sci. Rep.-UK*, 9, 1–11, 2019.

- Körtzinger, A., Mintrop, L., Wallace, D. W., Johnson, K. M., Neill, C., Tilbrook, B., Towler, P., Inoue, H. Y., Ishii, M., and Shaffer, G.: The international at-sea intercomparison of  $f\text{CO}_2$  systems during the R/V *Meteor Cruise 36/1* in the North Atlantic Ocean, *Mar. Chem.*, 72, 171–192, 2000.
- Landschützer, P., Laruelle, G. G., Roobaert, A., and Regnier, P.: A uniform  $p\text{CO}_2$  climatology combining open and coastal oceans, *Earth Syst. Sci. Data*, 12, 2537–2553, <https://doi.org/10.5194/essd-12-2537-2020>, 2020.
- Laruelle, G. G., Dürr, H. H., Slomp, C. P., and Borges, A. V.: Evaluation of sinks and sources of  $\text{CO}_2$  in the global coastal ocean using a spatially-explicit typology of estuaries and continental shelves, *Geophys. Res. Lett.*, 37, L15607, <https://doi.org/10.1029/2010GL043691>, 2010.
- Laruelle, G. G., Lauerwald, R., Pfeil, B., and Regnier, P.: Regionalized global budget of the  $\text{CO}_2$  exchange at the air-water interface in continental shelf seas, *Global Biogeochem. Cy.*, 28, 1199–1214, 2014.
- Laruelle, G. G., Goossens, N., Arndt, S., Cai, W.-J., and Regnier, P.: Air–water  $\text{CO}_2$  evasion from US East Coast estuaries, *Biogeosciences*, 14, 2441–2468, <https://doi.org/10.5194/bg-14-2441-2017>, 2017a.
- Laruelle, G. G., Landschützer, P., Gruber, N., Tison, J.-L., Delille, B., and Regnier, P.: Global high-resolution monthly  $p\text{CO}_2$  climatology for the coastal ocean derived from neural network interpolation, *Biogeosciences*, 14, 4545–4561, <https://doi.org/10.5194/bg-14-4545-2017>, 2017b.
- Laruelle, G. G., Cai, W.-J., Hu, X., Gruber, N., Mackenzie, F. T., and Regnier, P.: Continental shelves as a variable but increasing global sink for atmospheric carbon dioxide, *Nat. Commun.*, 9, 454, <https://doi.org/10.1038/s41467-017-02738-z>, 2018.
- Lefèvre, N., Diverriès, D., and Gallois, F.: Origin of  $\text{CO}_2$  undersaturation in the western tropical Atlantic, *Tellus B*, 62, 595–607, 2010.
- Li, D., Chen, J., Ni, X., Wang, K., Zeng, D., Wang, B., Jin, H., Huang, D., and Cai, W. J.: Effects of Biological Production and Vertical Mixing on Sea Surface  $p\text{CO}_2$  Variations in the Changjiang River Plume During Early Autumn: A Buoy-Based Time Series Study, *J. Geophys. Res.-Oceans*, 123, 6156–6173, 2018.
- Litt, E. J., Hardman-Mountford, N. J., Blackford, J. C., Mitchelson-Jacob, G., Goodman, A., Moore, G. F., Cummings, D. G., and Butenschön, M.: Biological control of  $p\text{CO}_2$  at station L4 in the Western English Channel over 3 years, *J. Plankton Res.*, 32, 621–629, 2010.
- Macklin, P. A., Maher, D. T., and Santos, I. R.: Estuarine canal estate waters: Hotspots of  $\text{CO}_2$  outgassing driven by enhanced groundwater discharge?, *Mar. Chem.*, 167, 82–92, 2014.
- Marrec, P., Cariou, T., Collin, E., Durand, A., Latimier, M., Macé, E., Morin, P., Raimund, S., Vernet, M., and Bozec, Y.: Seasonal and latitudinal variability of the  $\text{CO}_2$  system in the western English Channel based on Voluntary Observing Ship (VOS) measurements, *Mar. Chem.*, 155, 29–41, 2013.
- Mehrbach, C.: Measurement of the apparent dissociation constants of carbonic acid in seawater at atmospheric pressure, *Limnol. Oceanogr.*, 18, 897–907, 1973.
- Mellor, G. L. and Yamada, T.: Development of a turbulence closure model for geophysical fluid problems, *Rev. Geophys.*, 20, 851–875, 1982.
- Najjar, R. G., Herrmann, M., Alexander, R., Boyer, E. W., Burdige, D. J., Butman, D., Cai, W., Canuel, E. A., Chen, R. F., and Friedrichs, M. A.: Carbon budget of tidal wetlands, estuaries, and shelf waters of Eastern North America, *Global Biogeochem. Cy.*, 32, 389–416, 2018.
- Nightingale, P. D., Malin, G., Law, C. S., Watson, A. J., Liss, P. S., Liddicoat, M. I., Boutin, J., and Upstill-Goddard, R. C.: In situ evaluation of air–sea gas exchange parameterizations using novel conservative and volatile tracers, *Global Biogeochem. Cy.*, 14, 373–387, 2000.
- Orr, H., Des Clers, S., Simpson, G., Hughes, M., Battersbee, R., Cooper, L., Dunbar, M., Evans, R., Hanaford, J., and Hannah, D.: Changing water temperatures: a surface water archive for England and Wales, *Surface Water Temperature Archive [data set]*, <https://data.gov.uk/dataset/7b6b7515-3b63-4d70-9764-772e5823fdcc/surface-water-temperature-archive-up-to-2007> (last access: December 2016), 2010.
- Rees, A. P., Gilbert, J. A., and Kelly-Gerreyn, B. A.: Nitrogen fixation in the western English Channel (NE Atlantic ocean), *Mar. Ecol. Prog. Ser.*, 374, 7–12, 2009.
- Resplandy, L., Keeling, R., Rödenbeck, C., Stephens, B., Khatiwala, S., Rodgers, K., Long, M., Bopp, L., and Tans, P.: Revision of global carbon fluxes based on a reassessment of oceanic and riverine carbon transport, *Nat. Geosci.*, 11, 504–509, 2018.
- Ribas-Ribas, M., Anfuso, E., Gómez-Parra, A., and Forja, J. M.: Tidal and seasonal carbon and nutrient dynamics of the Guadalquivir estuary and the Bay of Cádiz (SW Iberian Peninsula), *Biogeosciences*, 10, 4481–4491, <https://doi.org/10.5194/bg-10-4481-2013>, 2013.
- Ribas-Ribas, M., Rérolle, V. M. C., Bakker, D. C. E., Kitidis, V., Lee, G. A., Brown, I., Achterberg, E. P., Hardman-Mountford, N. J., and Tyrrell, T.: Intercomparison of carbonate chemistry measurements on a cruise in northwestern European shelf seas, *Biogeosciences*, 11, 4339–4355, <https://doi.org/10.5194/bg-11-4339-2014>, 2014.
- Robbins, L., Daly, K., Barbero, L., Wanninkhof, R., He, R., Zong, H., Lisle, J., Cai, W. J., and Smith, C.: Spatial and temporal variability of  $p\text{CO}_2$ , carbon fluxes, and saturation state on the West Florida Shelf, *J. Geophys. Res.-Oceans*, 123, 6174–6188, 2018.
- Roobaert, A., Laruelle, G. G., Landschützer, P., Gruber, N., Chou, L., and Regnier, P.: The spatiotemporal dynamics of the sources and sinks of  $\text{CO}_2$  in the global coastal ocean, *Global Biogeochem. Cy.*, 33, 1693–1714, 2019.
- Santos, I. R., Maher, D. T., and Eyre, B. D.: Coupling automated radon and carbon dioxide measurements in coastal waters, *Environ. Sci. Technol.*, 46, 7685–7691, 2012.
- Shen, C., Testa, J. M., Li, M., Cai, W. J., Waldbusser, G. G., Ni, W., Kemp, W. M., Cornwell, J., Chen, B., and Brodeur, J.: Controls on carbonate system dynamics in a coastal plain estuary: A modeling study, *J. Geophys. Res.-Biogeo.*, 124, 61–78, 2019.
- Siddorn, J., Allen, J., and Uncles, R.: Heat, salt and tracer transport in the Plymouth Sound coastal region: a 3-D modelling study, *J. Mar. Biol. Assoc. UK*, 83, 673–682, 2003.
- Sims, R.: Richard-Sims/WCO\_tidal\_pco2: Processing code for WCO Tidal  $p\text{CO}_2$  paper (v1.0.0), Zenodo [code], <https://doi.org/10.5281/zenodo.6373406>, 2022.
- Sims, R. P., Schuster, U., Watson, A. J., Yang, M. X., Hopkins, F. E., Stephens, J., and Bell, T. G.: A measurement system for vertical

- seawater profiles close to the air–sea interface, *Ocean Sci.*, 13, 649–660, <https://doi.org/10.5194/os-13-649-2017>, 2017.
- Skamarock, W. C., Klemp, J. B., Dudhia, J., Gill, D. O., Barker, D. M., Wang, W., and Powers, J. G.: A description of the Advanced Research WRF version 3, NCAR Technical note-475 + STR, University Corporation for Atmospheric Research, <https://doi.org/10.5065/D68S4MVH>, 2008.
- Smagorinsky, J.: General circulation experiments with the primitive equations: I. The basic experiment, *Mon. Weather Rev.*, 91, 99–164, 1963.
- Smyth, T., Fishwick, J., Gallienne, C., Stephens, J., and Bale, A.: Technology, design, and operation of an autonomous buoy system in the western English Channel, *J. Atmos. Ocean. Tech.*, 27, 2056–2064, 2010a.
- Smyth, T. J., Fishwick, J. R., Lisa, A.-M., Cummings, D. G., Harris, C., Kitidis, V., Rees, A., Martinez-Vicente, V., and Woodward, E. M.: A broad spatio-temporal view of the Western English Channel observatory, *J. Plankton Res.*, 32, 585–601, 2010b.
- Takahashi, T., Sutherland, S. C., Wanninkhof, R., Sweeney, C., Feely, R. A., Chipman, D. W., Hales, B., Friederich, G., Chavez, F., and Sabine, C.: Climatological mean and decadal change in surface ocean  $p\text{CO}_2$ , and net sea–air  $\text{CO}_2$  flux over the global oceans, *Deep-Sea Res. Pt. II*, 56, 554–577, 2009.
- Torres, O., Kwiatkowski, L., Sutton, A. J., Dorey, N., and Orr, J. C.: Characterizing mean and extreme diurnal variability of ocean  $\text{CO}_2$  system variables across marine environments, *Geophys. Res. Lett.*, 48, e2020GL090228, <https://doi.org/10.1029/2020GL090228>, 2021.
- Torres, R., Artioli, Y., Kitidis, V., Ciavatta, S., Ruiz-Villarreal, M., Shutler, J., Polimene, L., Martinez, V., Widdicombe, C., and Woodward, E. M. S.: Sensitivity of modeled  $\text{CO}_2$  air–sea flux in a coastal environment to surface temperature gradients, surfactants, and satellite data assimilation, *Remote Sens.-Basel*, 12, 2038, <https://doi.org/10.3390/rs12122038>, 2020.
- Uncles, R. and Torres, R.: Estimating dispersion and flushing time-scales in a coastal zone: Application to the Plymouth area, *Ocean Coast. Manage.*, 72, 3–12, 2013.
- Uncles, R., Stephens, J., and Harris, C.: Estuaries of Southwest England: Salinity, suspended particulate matter, loss-on-ignition and morphology, *Prog. Oceanogr.*, 137, 385–408, 2015.
- Uncles, R., Clark, J., Bedington, M., and Torres, R.: On sediment dispersal in the Whitsand Bay Marine Conservation Zone: neighbour to a closed dredge-spoil disposal site, in: *Marine Protected Areas*, edited by: Humphreys, J. and Clark, R., Elsevier, Amsterdam, 599–629, 2020.
- Upstill-Goddard, R. C.: Air–sea gas exchange in the coastal zone, *Estuar. Coast. Shelf S.*, 70, 388–404, 2006.
- Van Heuven, S., Pierrot, D., Rae, J., Lewis, E., and Wallace, D.: MATLAB Program Developed for  $\text{CO}_2$  System Calculations, ORNL/CDIAC-105b, Carbon Dioxide Information Analysis Center, Oak Ridge National Laboratory, US Department of Energy, Oak Ridge, Tennessee, [https://cdiac.ess-dive.lbl.gov/ftp/co2sys/CO2SYS\\_calc\\_MATLAB\\_v1.1/](https://cdiac.ess-dive.lbl.gov/ftp/co2sys/CO2SYS_calc_MATLAB_v1.1/) (last access: 28 July 2016), 2011.
- Volta, C., Laruelle, G. G., and Regnier, P.: Regional carbon and  $\text{CO}_2$  budgets of North Sea tidal estuaries, *Estuar. Coast. Shelf S.*, 176, 76–90, 2016.
- Wanninkhof, R.: Relationship between wind speed and gas exchange over the ocean revisited, *Limnol. Oceanogr.-Meth.*, 12, 351–362, 2014.
- Ward, N. D., Bianchi, T. S., Medeiros, P. M., Seidel, M., Richey, J. E., Keil, R. G., and Sawakuchi, H. O.: Where carbon goes when water flows: carbon cycling across the aquatic continuum, *Frontiers in Marine Science*, 4, 7, <https://doi.org/10.3389/fmars.2017.00007>, 2017.
- Weiss, R. F.: Carbon dioxide in water and seawater: the solubility of a non-ideal gas, *Mar. Chem.*, 2, 203–215, [https://doi.org/10.1016/0304-4203\(74\)90015-2](https://doi.org/10.1016/0304-4203(74)90015-2), 1974.
- Widdicombe, C., Eloire, D., Harbour, D., Harris, R., and Somerfield, P.: Long-term phytoplankton community dynamics in the Western English Channel, *J. Plankton Res.*, 32, 643–655, 2010.
- Wolf, D. K., Shutler, J. D., Goddijn-Murphy, L., Watson, A., Chapron, B., Nightingale, P. D., Donlon, C. J., Piskozub, J., Yelland, M., and Ashton, I.: Key uncertainties in the recent air–sea flux of  $\text{CO}_2$ , *Global Biogeochem. Cy.*, 33, 1548–1563, 2019.
- Yang, M., Bell, T. G., Hopkins, F. E., Kitidis, V., Cazenave, P. W., Nightingale, P. D., Yelland, M. J., Pascal, R. W., Prytherch, J., Brooks, I. M., and Smyth, T. J.: Air–sea fluxes of  $\text{CO}_2$  and  $\text{CH}_4$  from the Penlee Point Atmospheric Observatory on the southwest coast of the UK, *Atmos. Chem. Phys.*, 16, 5745–5761, <https://doi.org/10.5194/acp-16-5745-2016>, 2016.
- Yang, M., Bell, T. G., Brown, I. J., Fishwick, J. R., Kitidis, V., Nightingale, P. D., Rees, A. P., and Smyth, T. J.: Insights from year-long measurements of air–water  $\text{CH}_4$  and  $\text{CO}_2$  exchange in a coastal environment, *Biogeosciences*, 16, 961–978, <https://doi.org/10.5194/bg-16-961-2019>, 2019.